Exchange reactions in metal-organic frameworks: New advances

Ming-Ming Xu, Qiang Chen, Lin-Hua Xie *, Jian-Rong Li *

Beijing Key Laboratory for Green Catalysis and Separation and Department of Environmental Chemical Engineering, Beijing University of Technology, Beijing 100124, P.R. China

ARTICLE INFO

ABSTRACT

There has been considerable interest and importance in using the "exchange reaction" to synthesize, modify, or functionalize metal-organic frameworks (MOFs), since the "exchange" can achieve desired changes in their structures and performances for various applications. In 2014, we published a critical review on this topic, in which the exchange of metal ions, ligands, and guests was discussed in detail. In the past five years, much progress has been made and some new and important results were published, which significantly promoted the development of MOF chemistry. In this review, the exchange reactions of the two main components of MOFs, namely metal center ions and ligands, are summarized based on the new results since 2014. The influence factors and processes of the exchange reactions are firstly discussed for guiding the design of functional MOFs. The lately reported works on exchange reactions of MOFs classified into two groups with seven subgroups are then introduced. Finally, a perspective is given, expecting that the exchange reactions will play a more and more important role in exploring novel or functional MOFs for applications in the future.

© 2020 Elsevier B.V. All rights reserved.

Contents

Abbreviations: MOF, metal-organic framework; ZIF, zeolitic imidazolate framework; MTV-MOFs, multivariate MOFs; ps-CMOF, porphyrin−salen chiral MOFs; SBU, secondary building unit; SBB, supermolecular building block; SC-SC, single crystal to single crystal; DRST, solvent-mediated dissolution and recrystallization crystal transformation; SALE, solvent-assisted linker exchange; USALE, ultrasonic-assisted linker exchange; 1,4-BPEB, 1,4-bis[2-(4-pyridyl)ethenyl]-benzene; 2-MIM, 2-methylimidazole; 2-NH$_2$-PZ, pyrazine-2-amine; 2-NIM, 2-nitroimidazolate; 3,4-H$_2$PyDC, 3,4-pyridine dicarboxylic acid; 4-ABPT, 4-amino-3,5-bis(4-pyridyl)-1,2,4-triazole; 4-BPDB, 1,4-bis(4-pyridyl)-2,3-diaza-1,3-butadiene; 4-BPMB, N^1, N^4-bis((pyridin-4-yl)-methylene)benzene-1, 4-diamine; 5-NBIM, 5-nitrobenzimidazole; AD, adeninate, AZP, 4,4′-azopyridine/1,2-di(pyridin-4-yl)diazene; BiPy, 4,4′-bipyridine; BPE, 4,4′-vinylenedipyridine; BPP, 1,3-bis(4-pyridyl)-propane; BPPCOOH, 2,6-bis(pyrazol-1-yl)pyridine-4-carboxylic acid; BPyE, 1,2-bis(4-pyridyl)ethylene); BTX, 1,4-bis(triazol-1-ylmethyl)benzene; DABCO, 4-diazabicyclo[2.2.2]octane; DPyB, 1,4-di(pyridin-4-yl)benzene; H$_2$(CH$_3$O)$_2$-TPDC, 2′,5′-dimethoxyterphenyl-4,4′′-dicarboxylic acid; H$_2$AZDC, azobenzene-4,4′-dicarboxylic acid; H$_2$BDC, 1,4-benzenedicarboxylic acid; H$_2$BPDC, biphenyl-4,4′-dicarboxylic acid; H$_2$BPYDC, 2,2′-bipyridne-5,5′-dicarboxylic acid; H$_2$CBAB, 4-carboxybenzylidene-4-aminobenzoic acid; H$_2$CPN, 6-(4-carboxyphenyl)-2-naphthoic acid; H$_2$FM, fumaric acid; H$_2$IPA, isopthalic acid; H$_2$Me$_2$BPDC, 2,2′-dimethylbiphenyl-4,4′-dicarboxylate; H$_2$NDC, 2, 6-naphthalenedicarboxylic acid; H$_2$NH$_2$BDC, 2-amino-1, 4-benzenedicarboxylic acid; H$_2$NO$_2$-eTPDC, 4-(3′-nitro-4′-(4′′-carboxylphenylethynyl)phenyl)benzoic acid; H$_2$NO$_2$-TPDC, 2′-nitro-1,1′:4′, 1′′- terphenyl-4,4′′-dicarboxylic acid; H$_2$OBA, 4,4′-oxybisbenzoic acid; H$_2$PyMLB, 4-Hydroxy-3-(((pyridin-2-yl)methylimino)methyl) benzoic acid; H$_2$TMBDC, Tetramethylterephthalic acid; H$_2$TPDC, p-terphenyl-4,4′′-dicarboxylic acid; H$_3$ABTC, 1-aminobenzene-3,4,5-tricarboxylic acid; H$_3$BTB, 1,3,5-benzenetribenzoic acid; H$_3$BTC, 1,3,5-benzenetricarboxylic acid H$_3$CAIP 5-(4-carboxybenzoylamino)-isophthalic acid; H$_3$TCBPA, tris(4′-carboxybiphenyl)amine; H$_3$TPTC, [1,1′:3′,1′′-terphenyl]-4,4′′,5′-tricarboxylic acid; H$_4$BDPI$^+$Cl$^-$, 1,3-bis-(3,5-dicarboxyphenyl) imidazoliumchloride; H$_4$TADP, 5,5′-(1H-2,3,5-triazole-1,4-diyl)diisophthalic acid; H$_4$TMBDI, 2,3,5,6-tetramethyl-1,4-diisophthalic acid; H$_5$DPN, (2,5-di(3,5-dicarboxylphenyl)-nicotinic acid; H$_6$BDCPO, N,N′-bis(2,4-dicarboxyphenyl)-oxalamide; IMPEO, 1,8-di((imidazol-2-ylmethylene)-1-phenylethanamine)octane; INA, isonicotinate; IrL^{2-}, [pentamethylcyclopentadienyl*Ir-(2,2′-bipyridine-5,5′-dicarboxylate)(Cl)Cl]$^{2-}$; Me$_3$MPBA^{4-}, N N′-2,4,6-trimethyl-1,3-phenylenebis(oxamate); NH$_2$BzIm, 2-aminobenzimidazole; NO$_2$Im, 2-nitroimidazole; OAM, oleylamine; PhIm, 2-phenylimidazole; PyINA, (pyridin-4-yl)isonicotinamide; PZ, pyrazine; S(R)-OH-BIM, S(R)-2-(1-hydroxyethyl)benzimidazole; SHBzIm, 2-mercaptobenzimidazole; TCAT, thiocatecholate; TTR4A, 1,2,4-triazol-ylmethylresorcin[4]arene; DCM, dichloromethane; DEF, dimethylformamide; DMA, N,N-dimethylacetamide; DMF, N, N-dimethylformamide; EtOH, ethanol; Me$_2$CO$_3$, dimethylcarbonate; MeCOOH, acetic acid; MeOH, methanol; Py, pyridine; THF, tetrahydrofuran; SEM, scanning electron microscopy; SCXRD, single-crystal X-ray diffraction; PXRD, powder X-ray diffraction; EDS/EDX, energy dispersive X-ray spectroscopy; ICP-AES, inductively coupled plasma-optical atomic emission spectrometer; FT-IR, Fourier transform infrared spectroscopy; NMR, nuclear magnetic resonance; XPS, X-ray photoelectron spectroscopy.

* Corresponding authors.

E-mail addresses: xielinhua@bjut.edu.cn (L.-H. Xie), jrli@bjut.edu.cn (J.-R. Li).

1. Introduction

Metal-organic frameworks (MOFs) [1–7] have garnered significant interest over the past two decades due to their promising potential in many applications such as gas adsorption [8], separation [9–11], catalysis [12–14], and sensing [15,16]. Compared with other porous materials such as zeolites and mesoporous silicas, MOFs could be more facilely designed and functionalized by the judicious choice of building units (metal ions/clusters and organic ligands) or post-synthetic modifications owing to their tunability on the molecular scale [3,17,18]. However, the precise control of MOF structures and their functionalization is not always feasible in most cases because there are many factors (reaction temperature, solvent, reactant concentration, etc.) that could affect the assembly processes of their starting reactants [19]. The exchange reactions of the main components of MOFs, namely metal ions and ligands, provide an alternative and promising route to prepare desirable functional MOFs which may be not available by direct synthesis [20,21]. In such a reaction, the parent MOF as a template is added to a system of the external metal ions or ligands and then allows the exchange proceed [21]. Compared with traditional one-pot synthetic approach, the exchange reaction is beneficial for the control of the structure and property of target MOFs to some extent [22,23].

The exchange reactions of MOFs are usually achieved through two exchange processes/manners, the so-called solvent-assisted SC-SC transformation (a solid–liquid reaction) [24] and the solvent-mediated DRST (Scheme 1) [25]. Although both SC-SC transformation and DRST involve the processes of breaking and reforming coordination bonds, the framework topologies of MOFs during the SC-SC processes usually keep while change in the DRST processes in some cases. Generally, the formation of more stable coordination bonds is the main inherent driving force for the exchange reactions of MOFs, and smaller space potential resistance is favorable for the occurrence of exchange reaction [26]. In addition, the exchange ratio and degree can be controlled by adjusting experimental parameters, such as the solvent used, reaction temperature, duration, and the concentration of external metal ions or ligands [27–29].

Exchange reactions not only lead to the structural change of MOFs [30], but also serve as a way to enhance the performances
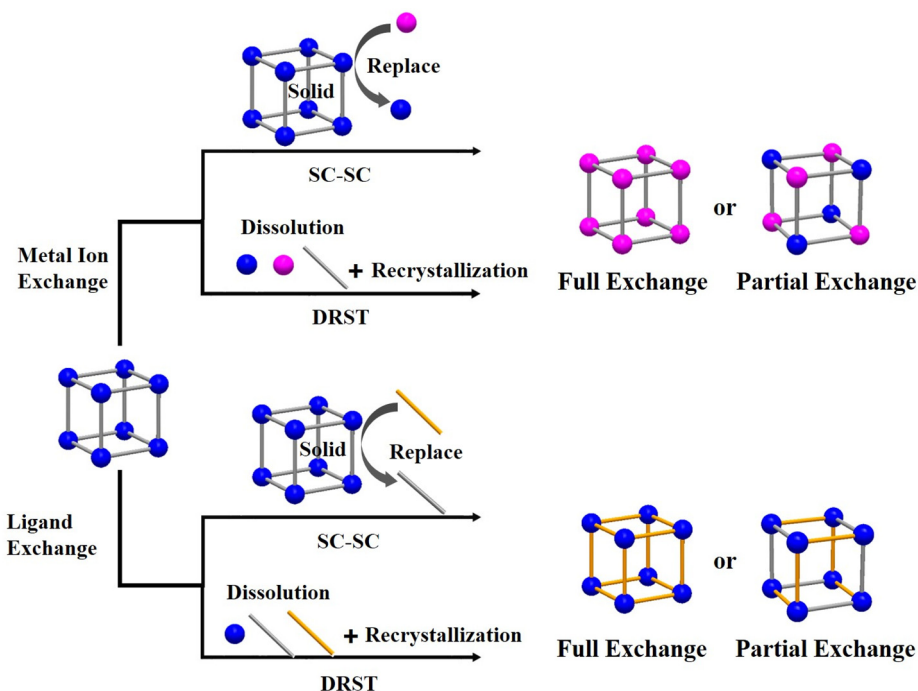

Scheme 1. Two common manners (SC-SC and DRST) of exchange reactions: metal ion and ligand exchanges in MOFs (Although specific example of metal ion exchange in DRST manner was not reported, it may appear in the future exploration).

of MOFs for various applications by modifying their compositions (metal centers and ligands) [31,32] or by adjusting their structural characteristics (e.g. pore size, shape, and surface) [22,23,33–36]. It was found that the exchange of metal ions could 1) strengthen the stability of MOFs through introducing metal centers with stronger coordination bonding with the ligands [37], 2) improve adsorption [38], separation [39] and/or catalysis performances [40] of MOFs through introducing open metal sites, 3) enhance the fluorescence emission of primary MOF through the incorporation of fluorescent metal ions (typically rare-earth ions) [41], 4) tune the magnetic properties of MOFs through introducing metal centers with different electronic structures [42]. For the ligand exchange reactions, 1) hydrophobic groups can be introduced to protect coordination bonds, thereby improving the water stability of MOFs [43], 2) specific functional groups (such as amino group, mercapto group, etc.) with the strong interaction with guest molecules can be introduced to improve the adsorption [44], separation [45] and/or catalysis performances [46] of MOFs, 3) special carriers (such as nitrogen atoms that can coordinate with palladium nanoparticles) can be installed into frameworks for the loading precious metals with catalytic activity [47], 4) fluorescent ligands with conjugated groups can be brought into the framework to enhance the fluorescence of MOFs [48].

Although several excellent reviews about post-synthetic modification of MOFs [34,49] and the construction of mixed-metal MOFs have been already published [50,51], there are relatively few reviews specifically focusing on the exchange reactions of metal ions or ligands in MOFs [20,21]. In 2014, we published a review that summarized the exchange reactions of metal ions, organic ligands, and free guest molecules in MOFs [20]. Recently, Sun's group published a review on postsynthetic exchange and the sequential linker installation in MOFs [21], however, only an overview of the post-synthetic methods was present, the changes in the structure and property of MOFs after post-modification were not specifically discussed in the work. In addition, to the best of our knowledge, the influencing factors and processes of exchange reactions in MOFs have not been proposed and discussed in the reported review papers. Following our previous review [20], in this contribution, we update and summarize the new progress on the exchange reactions in MOFs achieved in the past five years, mainly focusing on the metal ions and ligands exchanges. The processes and influencing factors of exchange reactions are firstly analyzed and summarized in detail. Then, the reported examples (Table A.1 and Table A.2, see Supporting Information) with structure tuning and property modification based on metal ion or ligand exchange reactions are classified and discussed in accordance with the chapters, so as to provide meaningful references for researchers in designing, synthesizing, and functionalizing MOFs for various applications.

2. The influencing factors and processes of exchange reaction

There are many factors influencing the exchange reactions of MOFs, including the nature of original and incoming metal ions and ligands, the characteristics of associated coordination bonds, and the pore structures of MOFs (Scheme 2) [52]. Four main aspects should be taken into consideration for a metal ion exchange reaction [40,52,53]. 1) The first coordination sphere of original metal ion. In some MOFs, the metal ions are coordinated with one or more solvent molecules, or coordinated with a ligand with a weak binding energy. The steric hindrance is relatively low for an ion exchange reaction of such metal ions, including some single metal nodes, the metal sites of some rod-shaped SBUs [37,54], the metal sites of dimeric paddle-wheel SBUs with labile water molecules occupying their apical positions [31]. 2) The similarity in coordination preference of the original and incoming metal ions. Successful metal ion exchange reactions commonly occur for the metal ions sharing similar coordination number and coordination geometry. 3) The thermodynamic stability of SBUs. Commonly, the thermodynamic stability of the daughter SBU and MOF is higher than that of the parent SBU and MOF. The formation of stronger coordination bonds and more stable MOFs is the thermodynamic driving force of exchange reactions [49,55–57]. The stability of coordination bonding of a certain ligand and divalent first-row transition metal ions was found to be in the order of Cu(II) > Zn(II) > Co(II) ≈ Ni(II), which is consistent with the Irving–Williams series [53]. 4) The diffusibility of the incoming metal ions in the interior of original MOF. Freely entering the interior of the MOF of the incoming metal ions is necessary for a metal ion exchange reaction with high conversion. In other words, the mass transfer is an important factor affecting the process of exchange reactions [42,58]. There are also four main aspects affecting the ligand exchange reactions. 1) The coordination groups and connectivity of incoming and original ligands. The incoming ligands commonly have the same coordination groups and connectivity of the original ligands in ligand exchange reactions, except the cases where the coordinated solvent molecules in the parent MOFs were exchanged by new ligands. 2) The connectivity of original ligand. Generally, the connectivity of ligands of parent MOFs in the existing ligand exchange reactions is mostly two, with few cases being three [48] or four [125]. The exchange process should be more difficult for the linker with higher connectivity, due to the requirement of more steps for the dissociation of original ligands. 3) The pK_a of incoming ligands. In most cases, the ligands (such as carboxylic acids, and azoles) need be deprotonated to coordinate with metal ions. The deprotonation of incoming ligands has a direct impact on the rate and extent of ligand exchange reactions [59,60]. Low pK_a values of incoming ligands kinetically facilitate
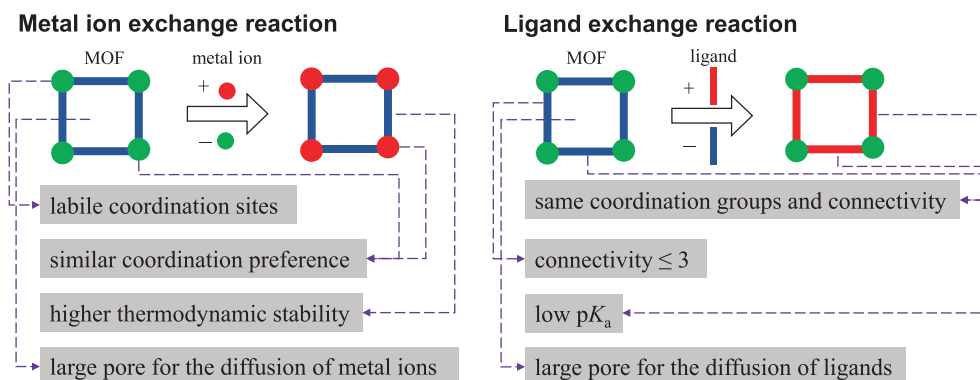
Scheme 2. General guiding principles for exchange reactions of MOFs.

the ligand exchange reactions, although it is well accepted that the MOFs synthesized from low pK_a ligands are thermodynamically less stable than those synthesized from high pK_a ligands [43]. 4) The diffusibility of the incoming ligands in the interior of original MOF. The pores of parent MOFs need be sufficiently large for facilitating the ligand diffusion [61].

Although many aspects described above about essential factors are important for the successful exchange reactions, sometimes these limits from MOF composition and structure can be overcome by regulating reaction conditions (external factors). The external factors include the solvent where the exchange reaction takes place, solution concentration of incoming ions or ligands, the temperature and the exchange reaction duration [27,39]. The effect of solvent on exchange reactions has been investigated in some works [28,62,63]. For example, the as-synthesized [Zn$_2$(TMBDI)(H$_2$O)$_2$]$_n$ (**UPC-6**) and [Co$_2$(TMBDI)(DMA)$_2$]$_n$ (**UPC-8**) by Xiao and co-workers were immersed different Cu^{2+} solvents (DMF, 1:1 DMF/CH$_3$OH mixture and CH$_3$OH) for 3d, respectively. The results showed that the ratios of Co^{2+} in **UPC-8** exchanged by Cu^{2+} were 1%, 12%, and 99%, respectively. For **UPC-6**, 53% Zn^{2+} were exchanged by Cu^{2+} in CH$_3$OH, while no obvious exchange was observed in the DMF and DMF/CH$_3$OH. These results indicated that the size of the solvated metal ions could affect the diffusion of metal ions into the channels of MOFs [64]. It was confirmed in the example of metal ion exchange reaction from {[Zn$_3$(TPTC)$_2$(DABCO)(H$_2$O)]·9DMF} into a isostructural Zn(II)-Cu(II) hybrid framework that the higher the concentration of the outside metal ions or ligands is, the faster the metal ion metathesis proceeds [54]. During the exchange process, the replacement of the solution of metal ions or ligands with fresh one at a certain frequency can drive the reaction forward to a higher conversion degree [38,65].

The influence of the reaction temperatures on the metal metathesis process was investigated through the exchange reaction metioned above from **NPC-7-Zn** to **NPC-7-Cu**. The results showed that high temperature can solve the kinetic issues induced by constricted pores [52]. However, the framework structure of MOF may be destroyed if the reaction temperature increases to a certain extent. Therefore, it is necessary to choose a balanced temperature to speed up the exchange reaction rate but ensure the crystallinity of MOF during the exchange process. It is also well-accepted that before reaching equilibrium, the longer the reaction duration is, the greater the exchange ratio is [37]. External factors play an important role in metal ion exchange, which provides important information for future study on exchange reactions for MOFs. Various exchange rates and degrees can be controlled by regulating these conditions, thus forming partial or complete substitution products.

Two main manners based on different processes for the exchange reactions in MOFs, namely, the solvent-assisted SC-SC transformation [66] and the solvent-mediated DRST [67,68] were mentioned in the literature. In both of them, the proposed mechanisms involve the destruction and re-formation of coordination bonds. However, the SC-SC transformation takes place through a solid-state diffusion mechanism [66], but the DRST process involves the dissolution of the initial coordination polymer, followed by the formation and crystallization of a new coordination polymer from the solution phase [67,68]. In other words, the essential difference between the two transformation manners is that no crystal dissolution can be observed in SC-SC transformation process. An obvious evidence of SC-SC transformation is that the final crystals had the same size and shape as those of the original ones [69]. Metal ion and most ligand exchange reactions usually
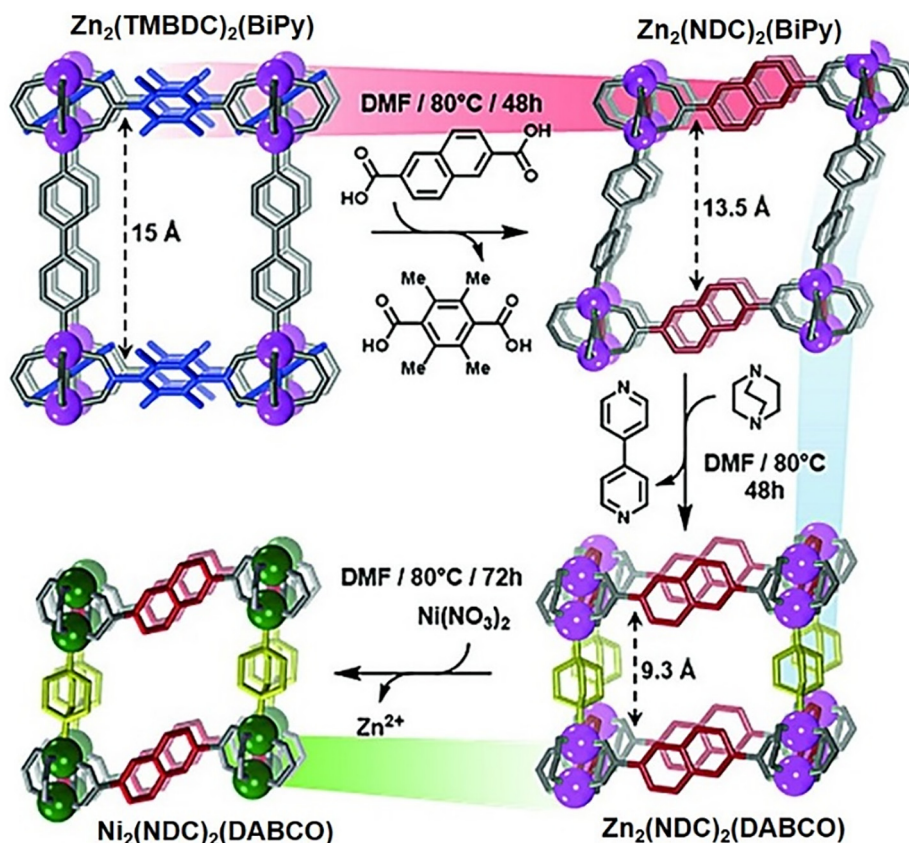

Fig. 1. The stepwise ligand and metal ion exchange reactions of Zn$_2$(TMBDC)$_2$(BiPy). Adapted with permission from Ref. [70].
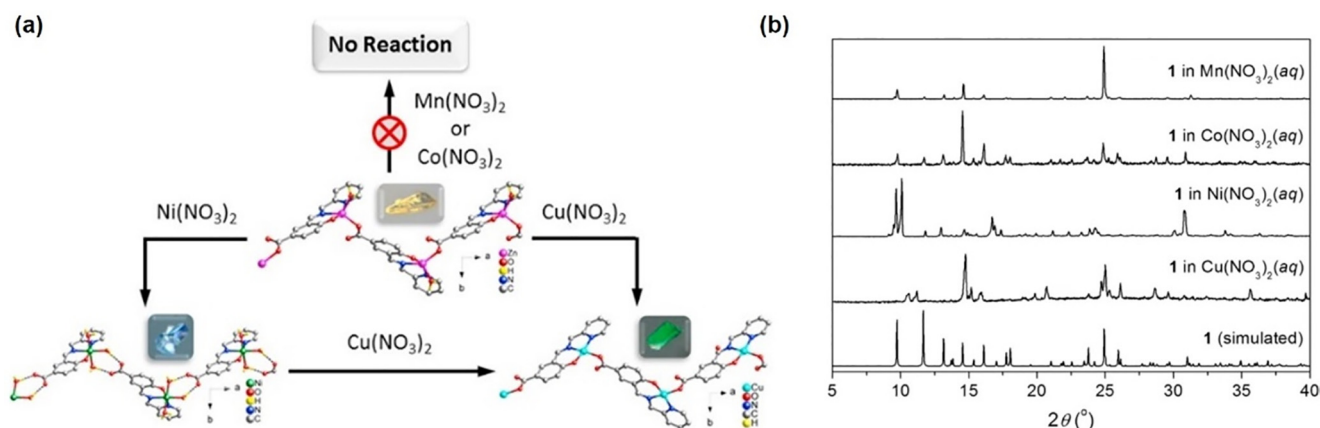
Fig. 2. (a) The structure transformation display among $[Zn(PyMLB)(H_2O)]_n$ (**1**), its exchange products **2** and **3**, (b) PXRD patterns of **1** (simulated) and its exchange products. Adapted with permission from Ref. [30].

undergo the SC-SC transformation during which the topology of the parent MOF generally is sustained [22,66], while only few ligand exchange reactions undergo the DRST process to complete structural rearrangement and form a favourable topology due to the different configuration characteristics between the outgoing and incoming ligand (such as from a ragid ligand to a flexible one) [25]. In addition, metal ion exchange and ligand exchange could occur in the same MOF in stepwise SC-SC transformations. For example, Farha's group reported a MOF obtained by both metal ion and ligand exchange reactions [70]. The MOF $Zn_2(TMBDC)_2$ (BiPy) with a aperture of 15 Å can convert into $Ni_{1.5}Zn_{0.5}(NDC)_2$ (DABCO) with a aperture of 9.3 Å (Fig. 1). The exchange process was carried out in three steps (1) carboxylate strut exchange producing $Zn_2(NDC)_2(BiPy)$, (2) nitrogen pillar exchange producing $Zn_2(NDC)_2(DABCO)$, and (3) metal ion transmetalation from Zn(II) to Ni(II). During these exchange processes, the topology of MOF framework remained unchanged, but the pore size and environment changed significantly.

The SC-SC transformation process was further developed in 2019 by introducing ultrasonic wave as extra driving force during one linker exchange reaction. The new method was called USALE. The transformation from **TMU-4** to **TMU-34** was chosen to study and compared the two methods, SALE and USALE [71]. It was found that under the same exchange conditions, it took less time for the USALE (2 h) than the SALE (52 h) method to achieve complete transformation from **TMU-4** to **TMU-34**. There are two reasons for the increase in exchange rate: (1) cavitation collapse can lead to faster removal of the original ligand from the framework, (2) the use of ultrasound wave makes the penetration of new ligands into the framework kinetically easier. Furthermore, the N_2 and CO_2 adsorption measurements showed that **USALE-TMU-34** exhibited a higher adsorption capacity than **SALE-TMU-34**, which was attributed to the linker-based defects inside the parent framework resulted from the fast removal of the original ligands. Compared with SALE, the USALE is a more effective method for ligand exchange for accelerating exchange rate and improving the adsorption capacity of MOFs.

Some characterization methods are commonly used to track the progress of exchange reactions. The change of crystal morphology can be visualized by SEM technology. The SCXRD can be used to the direct analysis of crystal structures of MOFs obtained through exchange reactions. It can be identified whether the crystal phase has been destroyed or changed through the PXRD measurement. The ratio of metal ion exchange can be calculated based on data obtained by EDS/EDX or ICP-AES, and the degree of ligand exchange can be verified by FT-IR and NMR spectra. The oxidation state of metal centers can be investigated by XPS measurement.

3. Exchange reactions of metal ions

Metal ions mainly exist in the metal cores (secondary building units, SBUs) and metalloligands in MOFs [26]. Herein, the exchange reactions of metal ions in the SBUs are discussed in detail according to their different metal valence states.

3.1. Low-valent (divalent) metal ion exchange

Based on the relatively weak coordination bonds between most of low-valent metal ions and organic coordination donors, divalent metal ions in some MOFs can be readily exchanged by some other metal ions with the same valence [33,36].

When the divalent metal ions in the SBUs of parent MOF are exchanged with those exhibiting the same coordination preferences, the topology of framework generally keeps unaltered during the process of metal ion exchange in MOFs. However, the coordination environment of metal ions in MOFs can be changed in coordination number and/or coordination geometry by the exchange reaction among those metal ions possessing various coordination geometries based on their different d-electron configurations. So, meanwhile, the chemical compositions of MOF crystals can also be designed as needed through metal ion exchange. For example, Wu and co-workers investigated the structural transformation of a flexible chain polymer through metal ion exchange [30]. The as-synthesized samples of $[Zn(PyMLB)(H_2O)]_n$ (**1**, 0.05 mmol) were soaked in aqueous solutions (4 mL) of $M(NO_3)_2 \cdot 6H_2O$ (M = Mn, Co, Ni, Cu; 0.05 mmol) at room temperature for 6 days. It was found that the products obtained from the Zn(II)-MOF samples exchanged with Ni^{2+} and Cu^{2+} aqueous solutions underwent an change in color (from bright-yellow to pale-blue and light-green, respectively) and crystal shape, but no change was observed for the samples exchanged with Co^{2+} and Mn^{2+} (Fig. 2a). Furthermore, PXRD patterns revealed the structure transformation of the original Zn(II)-MOF samples after being immersed in Ni^{2+} and Cu^{2+} aqueous solutions (Fig. 2b). SCXRD data analyses showed that the metal center adopted a 5-coordinated intermediate geometry of square pyramidal and trigonal bipyramidal in the original Zn(II)-MOF, while a 6-coordinated octahedral coordination geometry and a 4-coordinated square planar coordination geometry were found for metal ions in the resultant Ni(II)-MOF (**2**) and Cu(II)-MOF (**3**), respectively (Fig. 2a). The crystals of **2** and **3** can not be synthesized directly like **1**. These experimental results suggest that the metal ion exchange may serve as an efficient strategy of controlling the formation of MOFs with different coordination environment of metal centers. Based on the fact that different metal centers in
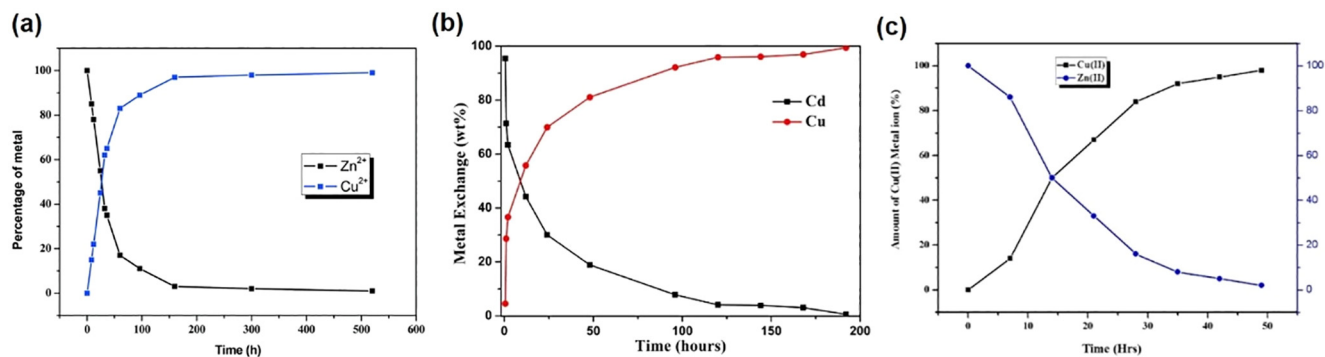
Fig. 3. The kinetic profiles of the metal ion exchange reactions in MOFs (a) [Zn$_3$CAIP$_2$(DMF)$_2$]·2DMF (**4**), (b) [Cd(TTR4A)(FM)]·2·.5H$_2$O (**6**), and (c) {Zn(BPPCOO)$_2$}$_n$ (**8**). Adapted with permission from Refs. [37,73,74].

MOFs have various coordination and connection numbers, more metal ion exchange reactions on metal centers can be further studied to adjust MOF structures.

In addition to changing the topological structures of MOFs, metal ion exchange can be used as a smart strategy of improving or changing MOF properties, such as stability [53], adsorption/separation performance [39], catalytic performance [72] and magnetism [42], etc.

High stability is necessary for many applications of MOFs. The exchange of parent metal ions in MOFs with others exhibiting stronger coordination ability is a feasible way to enhance the stability of MOFs. The trend of metal ion exchange is to produce thermodynamic stable MOF analogs of different metal ions with similar framework topology. For example, Zhao's group reported that the colorless crystals of a 3D MOF, [Zn$_3$CAIP$_2$(DMF)$_2$]·2DMF (**4**) soaked in a DMF/H$_2$O solution of Cu(NO$_3$)$_2$·3H$_2$O could transform into green–blue ones (**5**) at ambient temperature for 5 days with an exchange ratio of 97% [37]. The kinetics of the ion exchange process of Zn(II) with Cu(II) was monitored by ICP-AES as shown in Fig. 3a, while the structural maintenance of original MOF was confirmed by SCXRD and PXRD measurements. Furthermore, the exchange of Zn^{2+} ions in **4** with Ni^{2+} and Co^{2+} ions under the same condition was also investigated, and the results showed that Zn^{2+} ions could not be replaced by Ni^{2+} or Co^{2+} ions even after seven months. Similarly, Hu and co-workers synthesized a novel

capsule-like MOF, [Cd(TTR4A)(FM)]·2·.5H$_2$O (**6**), and explored its exchange reactions [73]. The as-synthesized colorless Cd(II)-MOF crystals could transform into a relatively stable blue Cu(II)-based compound (**7**) through metal-ion exchange in the solution (DMF/H$_2$O, v:v = 1:1) of CuCl$_2$·2H$_2$O for 3 days (Fig. 4). During the exchange of **6**, the degree of exchange process was further analyzed by ICP-AES as showed in Fig. 3b. However, the Cd(II) ions of the MOF soaking in solution of CoCl$_2$·6H$_2$O or NiCl$_2$·2H$_2$O could not be replaced by Co(II) or Ni(II) ions under the same condition since Cd(II)-based compounds are relatively stable with respect to the Ni(II)- or Co(II)-based counterparts. Recently, a similar example was reported by Bommakanti and co-workers [74], where a relatively stable MOF, {Cu(BPPCOO)$_2$}$_n$ (**9**) which was not synthesized directly, was obtained by metal ion exchange between {Zn(BPPCOO)$_2$}$_n$ (**8**) and Cu(II) ions in the solution of DMF at room temperature for 48 h. SCXRD and PXRD analyses of **9** showed that the **8** and **9** are isomorphous to each other. EDX spectroscopy studies indicated that the complete conversion took place and the kinetic plot is shown in Fig. 3c. However, the transmetalation reactions of {Zn(BPPCOO)$_2$}$_n$ with other metal ions (Mn(II), Fe(II), Co(II), and Ni(II)) did not show a change in crystal color, indicating nonoccurrence of metal ion exchange during the processes. Some other relatively stable Cu(II)-MOFs (**11** and **13**) can not being obtained directly through solvothermal synthesis also were obtained by similar metal ion exchange of parent Zn-MOFs, such as [Zn$_2$(4-
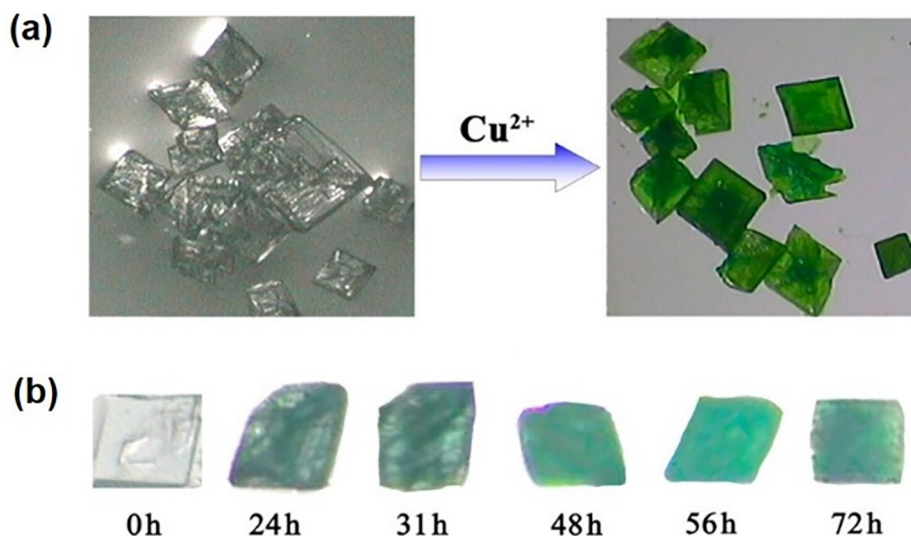

Fig. 4. (a) Photographs of crystals of [Cd(TTR4A)(FM)]·2·.5H$_2$O (**6**) and its Cu(II)-based compound (**7**) before and after metal-ion exchange (72 h). (b) Photographs of a single crystal of **6** taken during various immersion intervals after the exchange of Cd(II) with Cu(II). Reprinted with permission from Ref. [73].
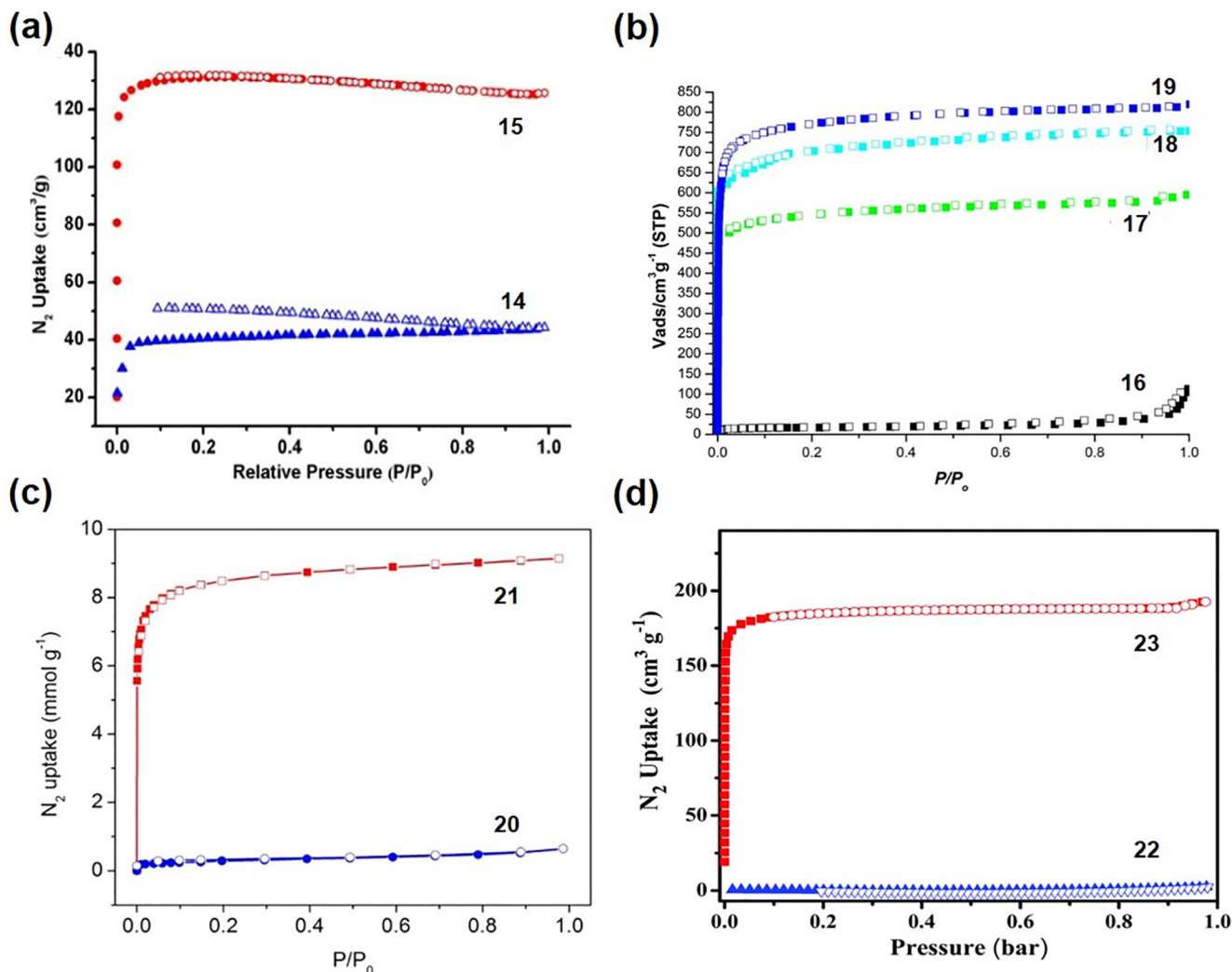
Fig. 5. N$_2$ adsorption patterns at 77 K of MOFs **SDU-1** (**14**), {[Zn$_3$(TPTC)$_2$(DABCO)(H$_2$O)]·9DMF} (**16**), **NCP-7-Zn**, (**20**), **NEM-7-Zn**, (**22**) and their metal ion exchange products, respectively. Adapted from with permission Ref. [38,39,52,54].

ABPT)(3,4-PyDC)$_2$]$_n$ (**10**) [53] and {Zn(OBA)(1,4-BPEB)$_2$}$_n$·nH$_2$O (**12**) [75]. In these metal ion exchange reactions, although the original MOFs only act as templates and their topologies keep unaltered, they change toward more stable structures, and the stability ordering corresponds to the Irving-Williams series [49,73].

The stability enhancement of MOFs through metal ion exchange can ensure their permanent porosity. Yang and co-workers

synthesized a Zn(II)-MOF (**SDU-1**, **14**) with two types of SBUs ([Zn$_2$(COO)$_3$] and [Zn$_2$(COO)$_4$]) and studied its metal ion exchange reactions and adsorption properties of the resultant MOFs [38]. The as-synthesized **SDU-1** possessed a very low N$_2$ adsorption caused by its inherent instability upon the removal of guest molecules. The Zn^{2+} ions in **SDU-1** were exchanged with Cu^{2+} ions from a DMF/EtOH/H$_2$O (v:v:v = 1:1:1) solution of CuCl$_2$ in a SC-SC fashion
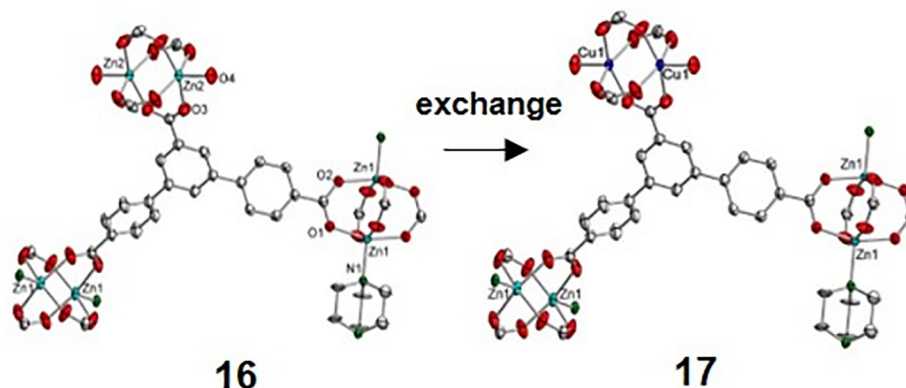

Fig. 6. View of the structures of MOFs {[Zn$_3$(TPTC)$_2$(DABCO)(H$_2$O)]·9DMF} (**16**) and its Cu(II) exchange product **17**. Adapted with permission from Ref. [54].
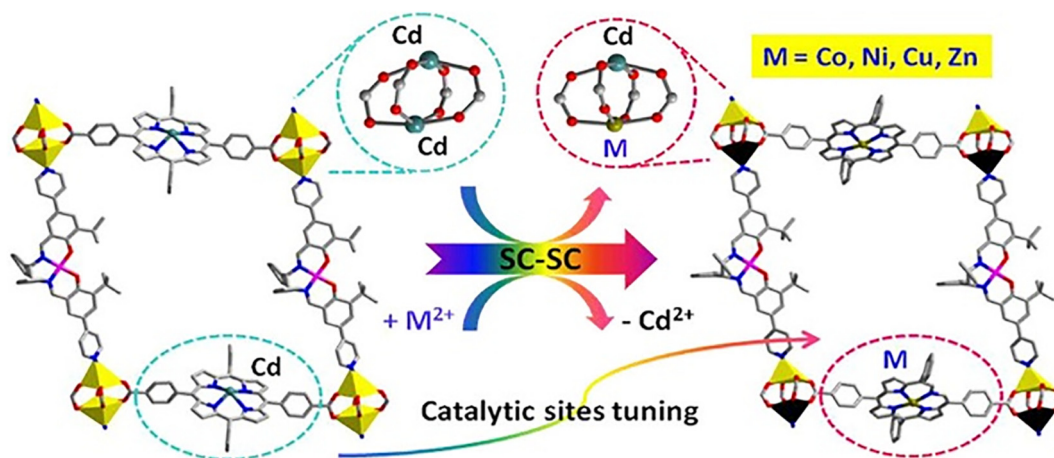
Fig. 7. (a) The process of metal ions exchange from **ps-CMOF 1** to **ps-CMOF 2–5**. Reprinted with permission from Ref. [40].

for 15 days, resulting in **Cu-SDU-1** (**15**). During the process, the CuCl$_2$ solution was replaced with a fresh one once a day to increase exchange rate. The N$_2$ adsorption measurements showed that the adsorption capacity of **Cu-SDU-1** was higher than that of **SDU-1** owing to its enhanced stability after metal ion exchange (Fig. 5a). Meanwhile, as catalyst in the reaction of the cyanosilylation of benzaldehyde and naphthaldehyde, **Cu-SDU-1** showed higher activity than **SDU-1** attributting to the enhanced stability. The enhancement of stability and adsorption performance via metal ion exchange was also demonstrated through a Zn(II)-MOF, {[Zn$_3$(TPTC)$_2$(DABCO)(H$_2$O)]·9DMF} (**16**), by Cui and co-workers [54]. The crystals of the Zn(II)-MOF soaked in a DMF solution of Cu(NO$_3$)$_2$ changed into an isostructural Zn(II)-Cu(II) hybrid framework (**17**) in the SC-SC manner at room temperature after 4 days with a substitution ratio of one-third. It is worth noting that the exchange ratio no longer changed at room temperature after the soaking time was prolonged. Fortunately, the diffraction data of **17** were successfully collected and the crystal structure was showed in Fig. 6. Only the Zn2 in the Zn(II)-MOF was exchanged by Cu(II). When the crystals of {[Cu$_3$(TPTC)$_2$(DABCO)(H$_2$O)]·9DMF} (**18**) synthesized directly were soaked into a DMF solution of Zn(NO$_3$)$_2$ for 5 days, another Cu(II)-Zn(II) hybrid compound (**19**) can be also obtained with a one-third exchange ratio. The N$_2$

adsorption of these activated compounds were shown in Fig. 5b. **16** showed only surface adsorption, **17**, **18** and **19** displayed typical type I adsorption isotherms and the maximum values were 590, 756 and 781 cm^3 g^{-1}, respectively. Compared with the original Zn(II)-MOF, the increased N$_2$ adsorption of **17** was attributed to the enhanced stability of the hybrid framework. More importantly, the two hybrid compounds could not be synthesized by the direct reactions of organic ligands with mixed zinc(II) and copper(II) salts. Li and co-workers obtained a relatively stable Cu$_{1.9}$Zn$_{0.1}$(TMBDI)(DMF)$_3$ (**NPC-7-Cu**, **21**) by repeated procedures (5 times) of solvothermal metal metathesis of constricted-pore containing Zn$_2$(TMBDI)(DMF)$_3$ (**NPC-7-Zn**, **20**) in a high concentration DMF solution of Cu(NO$_3$)$_2$ at 333 K for 24 h [52]. However, **21** could not obtained directly through solvothermal synthesis. The process was repeated for refreshing the DMF solution of Cu(NO$_3$)$_2$ to increase the exchange rate. From the N$_2$ adsorption measurements (Fig. 5c), it was found that **20** showed surface adsorption but **21** showed a typical type-I isotherm. Based on the saturated N$_2$ adsorption of **21**, its pore volume was calculated to be 0.317 cm^3 g^{-1} which was agreeable with the theoretical one of original Zn(II)-based MOF (0.314 cm^3 g^{-1}). In addition, the constricted pores of **21** led to high adsorbate density for CO$_2$ and CH$_4$ molecules, and a high CO$_2$/N$_2$ (simulated flue gases from power
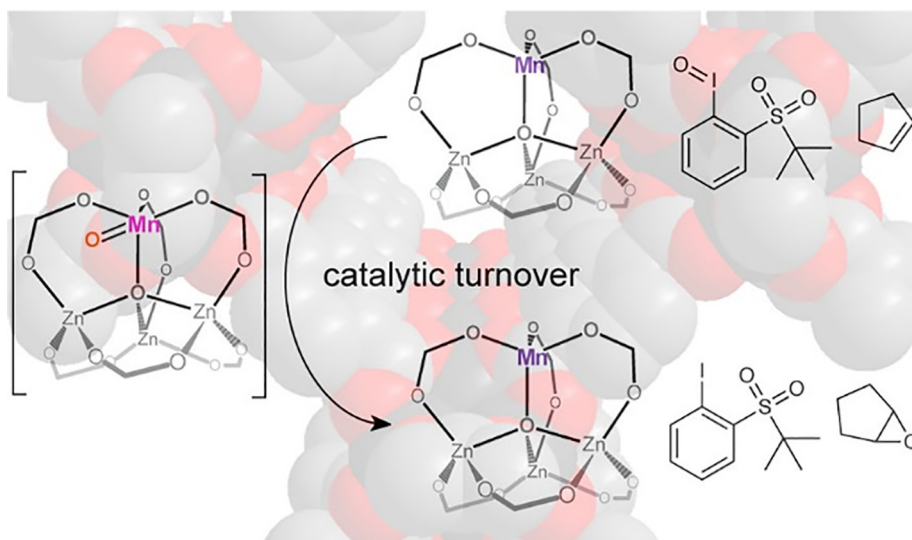

Fig. 8. The catalytic reaction process in the presence of ᵗBuSO$_2$PhIO and **Mn(II)-MOF-5** from cyclic alkenes to epoxides. Reprinted with permission from Ref. [72].

plants) selectivity of 30.2. In order to further explore this mechanism, the adsorption thermodynamic and kinetic studies were carried out. The analyses revealed that CH_4 and N_2 had faster diffusion rates than CO_2, and the surface diffusion barriers rather than molecular sieving effects in the constricted pores played the dominant role in the diffusion resistance. Later, Liu and co-workers reported a Cu(II)-MOF obtained through metal ion exchange for the separation of C_2/C_3 hydrocarbons [39]. Importantly, direct synthesis of the Cu(II)-MOF through the de novo synthesis using organic ligands and Cu(II) salts was unsuccessful. First, $[Zn_2(-DPN)\cdot(DMF)_3\cdot(CH_3)_2NH_2]\cdot(DMF)_2$ (**NEM-7-Zn**, **22**) was synthesized by a solvothermal reaction. Then, the as-synthesized crystals of **NEM-7-Zn** were soaked in a DMF/CH_3OH (v:v = 1:3) solution of $Cu(NO_3)_2$. The metal metathesis procedure was repeated six times at room temperature and the original colorless single crystals changed into blue ones (**NEM-7-Cu**, **23**) with a nearly complete transformation ratio, with only 2.7% Zn metal centers remained in the skeleton. N_2 adsorption experiment indicated that the framework of **NEM-7-Zn** collapsed after the removal of the guest molecules but that of **NEM-7-Cu** could adsorb 192 $cm^3 \ g^{-1}$ of N_2 under the same conditions (Fig. 5d). These results confirmed the improved stability of **NEM-7-Cu**. In addition, **NEM-7-Cu** was used for the separation of C_3H_6/C_2H_2, C_3H_8/C_2H_2, C_3H_6/C_2H_4, and C_3H_8/C_2H_4 (molar ratio: 10:90) and showed high calculated selectivities of 6.8, 7.1, 8.5, and 8.8 at 298 K, respectively. These separation results benefited from the enhanced stability, appropriate pore size, the uncoordinated $-COO^-$ and Lewis basic nitrogen sites on the pore surface of **NEM-7-Cu**. From these examples, it can be found that the metal ion exchange reactions open a new pathway for the synthesis of novel MOF materials with enhancing stability and outstanding adsorption/separation properties.

Metal ions, as the cores of MOFs, have significant effects not only on the framework stability to ensure their permanent porosity but also on the interactions between frameworks and guest molecules [39]. Thus, metal ion exchange can be considered as an effective method of introducing active metal sites into MOF framework to tune their adsorption/separation performance. Gallis and co-workers obtained the Mn(II), Fe(III), and Co(II) analogues of **Cu-BTC** (**24**) by metal ion exchange reactions and explored their gas (O_2 and N_2) adsorption performance [31]. The samples of **Cu-BTC** were added to DMF solutions of $MnCl_2\cdot4H_2O$, $FeCl_2\cdot4H_2O$, and $CoCl_2\cdot6H_2O$ to perform the metal ion exchange reactions at 90 °C for 1 day, respectively. About 6%, 13.5%, and 25.5% Cu^{2+} ions of **Cu-BTC** were replaced by the Mn(II), Fe(III), and Co(II) ions, respectively. Experimental O_2 and N_2 gas sorption isotherms of these compounds were measured at 77 K. Consistent for all samples studied, O_2 was more favorably adsorbed over N_2, with the O_2/N_2 adsorption selectivities at $0.2P/P_0$ as follows: 1.32 for **Mn/Cu-BTC** (**25**), 1.27 for **Fe/Cu-BTC** (**26**), 1.27 for **Co/Cu-BTC** (**27**), and 1.13 for **Cu-BTC**. The selectivities ranged from strong to weak in the order of Mn > Fe ≈ Co ≫ Cu, which was consistent with the trend established when considering the difference in O_2 and N_2 binding energies (ΔE) calculated from density functional theory (DFT). Experimental O_2 and N_2 isotherms were further measured at 273, 283, and 298 K and these data showed a good correlation with the Grand Canonical Monte Carlo (GCMC) simulated data. Different with other three metal-exchanged samples in that the amount of O_2 loading decreases with respect to N_2, the **Fe/Cu-BTC** sample showed similar O_2 and N_2 gas uptake due to its higher isosteric heat of adsorption for N_2 (~30 kJ/mol) than other samples (~15 kJ/mol) and the favorable interactions between N_2 and coordinatively unsaturated Fe metal centers.

Variable interactions between water molecules and the framework atoms could make MOFs hydrophilic or hydrophobic. The metal ion exchange can tune the hydrophilicity/hydrophobicity of MOFs through change the metal centers in the frameworks. As

Wright and co-workers reported [76], when the tetrahedral Zn^{2+} ions that are not known to bind additional solvent molecules to SBUs of **MFU-4l** were exchanged with five coordinate-accommodating Co^{2+} that can enable up to four water molecules binding to each SBU, the hydrophilicity of the parent MOF increased gradually although the total water adsorption capacity kept unaltered. The water uptake step can be precisely controlled in a range of 30% RH by tuning the metal ion exchange ratio. All these results indicate that metal ion exchange reactions provide a good way of improving the interaction between MOF frameworks and specific guest molecules to tune their adsorption/separation performance.

Besides adsorption sites, metal ion exchange also can introduce active catalytic sites into a serious of isostructural parent MOF analogues to tune their catalysis performance [72,77]. As Jiang's group reported [40], the crystals of **ps-CMOF 1** (**28**) were soaked in a DMF solution of MCl_2 (M = Cu, Zn, Ni, or Co) for 7 days, resulting in the new phase **ps-CMOF 2–5** (Fig. 7). In the process, crystal structures data revealed that the Cd(II) ions in the Cd_2 paddle-wheel node and in the center of the porphyrin moiety were replaced by the M(II) ions in 50% and 100%, respectively. The **ps-CMOF 5** (**29**) was chosen as a representative catalyst to evaluate the asymmetric catalytic performance. Different from the **ps-CMOF 1**, **ps-CMOF 5** could be utilized in the formation of cyclic carbonates from CO_2 and epoxides with a high efficiency and selectivity due to the presence of Co(II) sites. $Mn_{0.25}Zn_{3.75}(BDC)_3$ (**Mn(II)-MOF-5**, **31**) was obtained by Stubbs and co-workers through soaking **MOF-5** (**30**) in the DMF solution of $MnCl_2$ ($Mn(II):Zn_4O(BDC)_3$ = 4:1) at −35 °C for 7 days [72]. Partial substitution of **MOF-5** in the exchanging solution with low concentration of Mn(II) at low temperature is necessary to eliminate spin-spin interactions and ensure the structural stability and of the **MOF-5** framework. In fact, direct synthesis was more effective than postsynthetic cation exchange in the preparation of the more magnetically dilute Mn(II)-MOF-5 ($Mn_{0.026}Zn_{3.974}(BDC)_3$). The Mn(II) substituted product could catalyze the transfer of oxygen atoms and form epoxides from cyclic alkenes as showed in Fig. 8. During the catalytic process, Mn(II) ions in **Mn(II)-MOF-5** changed into Mn(IV)-oxo species in the presence of *tert*-butylsulfonyl-2-iodosylbenzene ($^tBuSO_2PhIO$), then Mn(IV)-oxo species further reacted with adventitious hydrogen to become Mn(III)-OH species. Similarly, compared with $CoFe_2O_4/Zn$-TMU-17-NH_2 (**32**), $CoFe_2O_4/[Cu_{0.63}/Zn_{0.37}$-TMU-17-$NH_2]$ (**33**) produced by Yadollahi and co-workers through metal ion exchange acted as a more effective catalyst for the production reactions of tetrazole derivatives via one-pot three-component reactions of different aldehydes with hydroxyl amine hydrochloride and sodium azide [78]. It is worth mentioning that **33** can not be synthesized through de novo synthesis. The research on isostructural MOFs is beneficial for determining the relationships between metal ions and the corresponding catalytic properties of MOFs. Wang and co-workers studied the exchange reactions of a Cd(II)-MOF, $\{[Cd_2(-TADP)(Py)_6]\cdot H_2O\}_n$ (**34**) and explored the different catalytic performances of **34** and the generated exchange products [79]. Under the similar conditions to synthesize **34**, all attempts of using divalent Cu(II), Co(II), and Ni(II) cations to directly synthesize MOFs were unsuccessful. Replacing the Cd(II) ions with Cu(II), Co(II), and Ni(II) ions through immersing the crystals of **34** in DMF solutions of $M(NO_3)_2$ (0.05 M) at 50 °C for 48 h. ICP-AES analyses revealed that 61%, 55%, or 8% of the Cd(II) ions were replaced by Cu(II), Co(II), or Ni(II) ions, respectively. Obviously, the exchange ratios were consistent with the stabilities of MOFs with different metal centers (Cu(II) > Co(II) ≫ Ni(II)). Then the original Cd(II)-MOF and the resultant Cu(II)-Cd(II)-, Co(II)-Cd(II)-, and Ni(II)-Cd(II)-MOF (**35**, **36** and **37**) were used to catalyze the cascade cyclization of 4-pyridyl nitriles with 1,3-diaminopropane for the production of 2-(pyridin-4-yl)-1,4,5,6-tetrahydropyrimidine. The catalytic

performance increased in the order of Cd(II)-MOF < Cu(II)-Cd(II)-MOF < Co(II)-Cd(II)-MOF < Ni(II)-Cd(II)-MOF, consistent with the expansion of their Lewis acid strengths which is related to electron accepting ability of the central-metal ions. In other words, the stronger is the Lewis acidity of the metal ion in the isostructural MOFs, the larger is the propensity of the metal ion to catalyze the production reaction of 1,4,5,6-tetrahydropyrimidine derivatives. These examples confirm that metal ion exchange can be utilized as a powerful alternative tool to prepare diverse frameworks with identical topologies with the original ones but improved catalytic performance.

MOFs are also used to separate some metal ions from liquid phase samples. It is regarded as a potential way to remove harmful metal ions in water by directly replacing the eco-friendly metal ions in MOFs with the harmful metal ions. Margariti and co-workers reported a related example [80]. The Ca^{2+} ions in [Ca(H$_4$-BDCPO)(DMA)$_2$]·2DMA (38) could be exchanged immediately by Cu^{2+} ions when the colorless crystals of Ca(II)-MOF ware immersed in an aqueous solution of [Cu$_2$(AcO$_2$)$_4$(H$_2$O)$_2$], CuCl$_2$·2H$_2$O, Cu(ClO$_4$)$_2$·6H$_2$O, Cu(BF$_4$)$_2$·6H$_2$O or Cu(NO$_3$)$_2$·3H$_2$O. Remarkably, the expensive ligand could be recycled by treating the Cu(II)-MOF with a dilute NaOH solution (0.1 M) followed by the addition of dilute HCl (3 M). These experimental results showed the potential of the Ca(II)-MOF for column ion-exchange to remove the Cu^{2+} from aqueous solutions.

Luminescent MOFs show great promise as various types of sensors based on their different degrees of luminescent enhancement or quenching in response to the interactions between included guest species and the framework [81]. Fluorescent MOFs can be obtained by selecting fluorescent metal ions as cores [54,82]. Metal ion exchange can be an alternative way to effectively tune the fluorescence of MOFs by changing the metal ions in SBUs. Huang and co-workers confirmed the effect of metal ion exchange in cores on the fluorescence signals of MOFs [81]. When the Cd(II) ions in the MOFs, [Cd(BTX)$_2$Cl$_2$]$_n$ (40) and {[Cd$_2$(BTX)$_2$(BDC)$_2$]•H$_2$O}$_n$ (42) were replaced by Co(II) or Cu(II) ions, the fluorescence signal of the two exchanged compounds was weakened, which was resulted from the quenching of ligand fluorescence emission by the paramagnetic ions. In contrast, the fluorescence signal could become stronger when the Co(II) ions in [Co(BTX)$_2$Cl$_2$]$_n$ (44) or [Co$_3$(BTX)$_4$(BDC)$_3$(H$_2$O)$_4$]$_n$ (46) were replaced by Cd(II) ions. In addition, Asha and co-workers obtained [Tb(H$_2$O)(BTB)] (49) with enhanced emission properties by immersing the crystals of [H$_2$N(CH$_3$)$_2$][Ba(H$_2$O)(BTB)] (48) in DMF solution of Tb(NO$_3$)$_2$·5H$_2$O for 24 h [41], and 49 could be used for selectively sensing phosphate anion in aqueous medium with a detection limit of 6.56 ppm. Synthesizing 49 through direct solvothermal reaction was unsuccessful. These examples illustrate that it is feasible to enhance the fluorescence properties of MOFs through replacing metal ions of MOF with the metals with d^{10} or 4f electronic configuration.

Magnetic MOFs (MMOFs) have attracted considerable attention in analytical chemistry and have been used in sample collection and pre-enrichment, solid-phase extraction, and solid-phase microextraction in recent years [83,84]. The magnetism of MOFs can be changed or adjusted by the metal ion exchange reactions. For example, two novel magnetic MOFs, Co$_2${Co$_4$[Cu$_2$-(Me$_3$MPBA)$_2$]$_3$}·56H$_2$O (51) and Ni$_2${Ni$_4$[Cu$_2$-(Me$_3$MPBA)$_2$]$_3$}·54H$_2$O (52) were synthesized by Grancha and co-workers through metal ion exchange of Mg$_2${Mg$_4$[Cu$_2$-(Me$_3$MPBA)$_2$]$_3$}·45H$_2$O (50) in the SC-SC manner [69]. During the metal ion exchange process, the framework structure remained unchanged, and only the diamagnetic Mg(II) ions in the original MOF were replaced by paramagnetic the Co(II) and Ni(II) ions, respectively, which caused the occurrence of a long-range magnetic ordering in 51 and 52. The spin-crossover (SCO) behaviors of certain metal ions can also be induced by the metal ion exchange processes. Zhang and co-workers have reported a related example [42] in which FeNi-1, −2, and −3 (54−56) were synthesized through soaking the [Ni$_4$(IMPEO)$_6$](BF$_4$)$_8$ (53) into the Fe^{2+} solution for 10 h, 2 days, and 5 days, respectively. The optical microscopic photographs of these compounds as shown in Fig. 9b–e (left) revealed the color change of 53 after metal ion exchange reactions. Magnetic property studies showed that the resulting FeNi cage exhibited SCO behaviors with the increase in the amount of Fe(II) ions, and the plots of $\chi_M T$ versus T for these compounds are showed in Fig. 9 (right). These results demonstrate the clear advantages of metal ion exchange reactions to obtain MOFs with predictable architectures as well as improved physical properties.
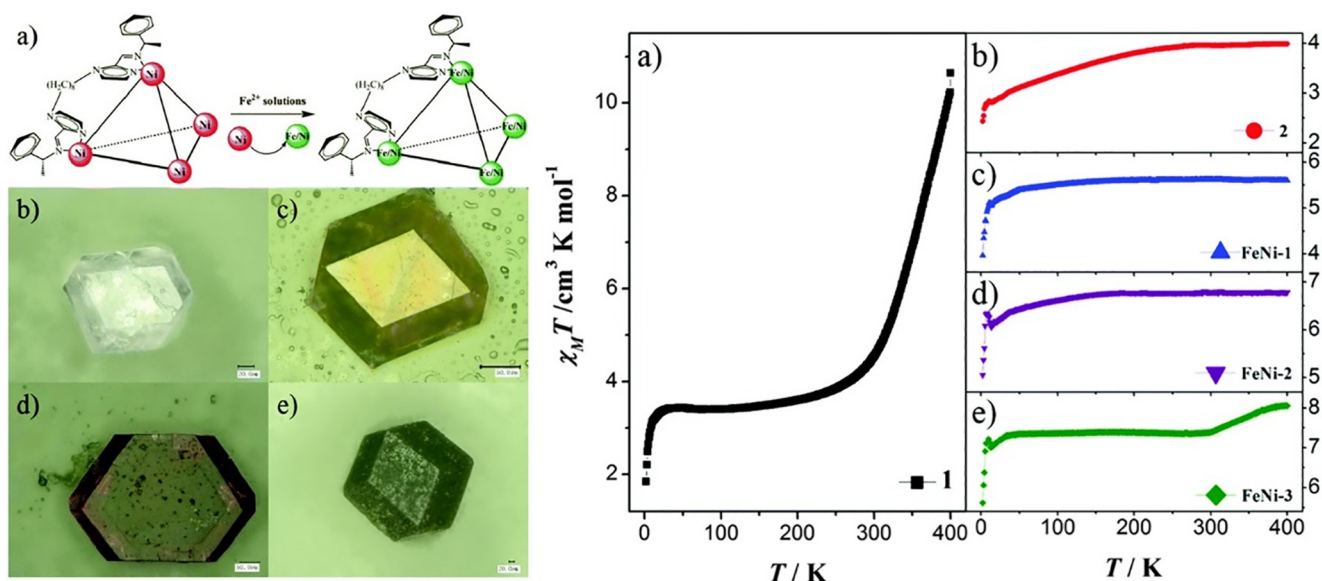

Fig. 9. Left: (a) The diagram of metal-center exchange from the Ni cage to the FeNi cage. Optical microscopic photographs of color change of SC-SC transformation in the metal-center exchange process (b) [Ni$_4$(IMPEO)$_6$](BF$_4$)$_8$ (53), (c) FeNi-1 (54), (d) FeNi-2 (55), and (e) FeNi-3 (56). Right: Plots of $\chi_M T$ versus T for (a) [Fe$_4$(IMPEO)$_6$](BF$_4$)$_8$, (b) 53, (c) 54, (d) 55, and (e) 56. Adapted with permission from Ref. [42].

3.2. High-valent (trivalent and tetravalent) metal ion exchange

High valence metal-containing (such as Fe^{3+}, Cr^{3+}, Zr^{4+}, and Ti^{4+}) MOFs have received increasing attention owing to their stronger metal–ligand coordination bonds and thus improved stability [4] compared with the MOFs composed of divalent metal centers. The stability of high valence metal-containing MOFs has been extensively demonstrated in the MIL, UiO and PCN-22X series MOFs [49,85]. Similar to low-valent metal ion exchange reactions in MOFs, the high-valent metal ion exchange also can be used to synthesize desired MOFs with improved properties.

The robust Cr(III)-MOFs obtained by one-pot method are rare, because the extreme kinetic inertness of the Cr(III)-O bond makes them trapped in the direct synthesis [86,87]. It is a promising strategy to construct the Cr(III)-MOFs through the metal ion exchange of Fe(III)-MOFs with Cr(III) ions, as the two types of metal ions are exhibiting the similar charge, radius, and coordination geometry. In 2015, Zhou's group reported a reductive labilization–metathesis route for the construction of **PCN-333-Cr(III)** from **PCN-333-Fe(III)** [88]. The vial containing a mixture of anhydrous $CrCl_2$, **PCN-333-Fe(III)** and DMF was heated at 85 ℃ for about 30 min until all of the solids turned green then to form **PCN-333-Cr(III)** (Route A of Fig. 10a). During the process, the Fe(III) ions in the framework were first reduced to Fe(II) ions, the Cr(II) ions of $CrCl_2$ then replaced the Fe(II) ions in **PCN-333-Fe(II)** (**57**), and the Cr(II) ions in the **PCN-333-Cr(II)** (**58**) were oxidized to Cr(III) ion at last. This synthetic route suffers from some shortcomings including harsh reaction conditions and complex reaction steps. Then, the same group obtained **PCN-333-Cr(III)** via direct metal ion exchange of **PCN-333-Fe(III)** in the DMF solution of $CrCl_3·6H_2O$ (Route B of Fig. 10a) [65], but the reaction must be carried out at high temperature (150 ℃). In addition, the reaction must be stopped shortly afterward in order to replace the solution with a fresh DMF solution of $CrCl_3·6H_2O$ to improve the exchange rate and increase the exchange degree. Later, Zhang's group reported the approach of solvent-assisted metal metathesis to obtain a series of **Cr(III)-MOFs** (**60**, **62**, **64**, **66**, **68**, and **70**) from a variety of **Fe(III)-MOFs** (**59**, **61**, **63**, **65**, **67**, and **69**) through the judicious selection of a solvent for the metal ion exchange reaction (Fig. 10b) [89]. In the study, various amide and ketone solvents were used and compared. The results showed that acetone was a promising solvent for the metal metathesis, and it could be used to construct a range of Cr(III)-MOFs under relatively low temperature (<100 °C) and a low Cr(III) concentration in a short period time (<24 h).
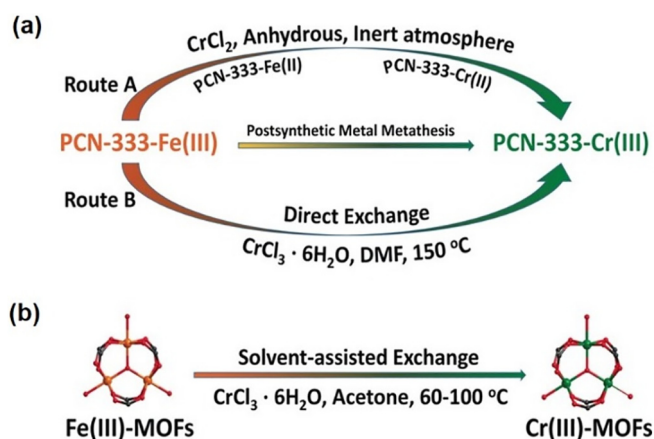
The authors pointed out that the coordination of the carbonyl group of the solvent to the metal ions played a vital role in the metathesis process. This work suggests that the selection of solvents is a key in the substitution reaction. At the same time, a highly efficient and versatile approach to obtain Cr-MOFs was developed.

Based on fluorescence quenching in response to the target ions, high-valent MOFs also can be used as various sensors. In addition to competitive excitation light absorption between MOFs and analytes and energy resonance transfer from the MOFs to the analytes [90–92], the fluorescence quenching effect of MOFs can also be induced by metal ion exchange. Yang and co-workers reported the first example for fluorescent sensing of Fe^{3+} in aqueous solution with a detection limit of 0.9 μM based on the metal ion replacement between the target Fe^{3+} ions and the Al^{3+} centers in **MIL-53(Al)** [93]. The fluorescence quenching of **MIL-53(Al)** (**71**) occurred because the resultant **MIL-53(Fe)** (**72**) obtained by ion exchange exhibited relatively weak fluorescence. Later, in another work, **Eu³⁺@MIL-53(Al)** was obtained by soaking **MIL-53(Al)** in the ethanol solutions of chlorate salt of Eu^{3+}, and the resultant new material was also used to detect Fe^{3+} ions in aqueous solution [94]. The detection limit of **Eu³⁺@MIL-53(Al)** (0.5 μM) was lower than that of **MIL-53(Al)** (0.9 μM), but the mechanism of luminescence quenching for the Eu^{3+} incorporated material was the same as that of original MOF, which was based on the exchange of Al^{3+} in the framework with the Fe^{3+} ions. The emission spectra of **Eu³⁺@MIL-53(Al)** and **Eu³⁺@MIL-53(Fe)** are shown in Fig. 11. In addition, diffuse-relectance UV–visible spectrum study implied that the cation exchange process needed consume some energy, which effectively suppressed the energy migration of excitation energy to Eu^{3+} and therefore caused luminescence quenching of **Eu³⁺@MIL-53(Al)**.

MOFs have shown their great potential as a new type of photocatalysts [95]. Introduction of metal-to-metal charge transfer mediator by metal cation exchange to construct metal-doping MOFs can bring about their enhanced photocatalytic performance [96–98]. Ti-substituted **NH₂-Uio-66(Zr)** (**73**) was prepared by Sun and co-workers through metal ion exchange at 100 °C for 4 days with a substitution ratio of 34.2% (57%) [99]. **NH₂-Uio-66 (Zr/Ti)** (**74**) showed an enhanced photocatalytic activity for the CO_2 reduction to $HCOO^−$ under visible-light irradiation. The
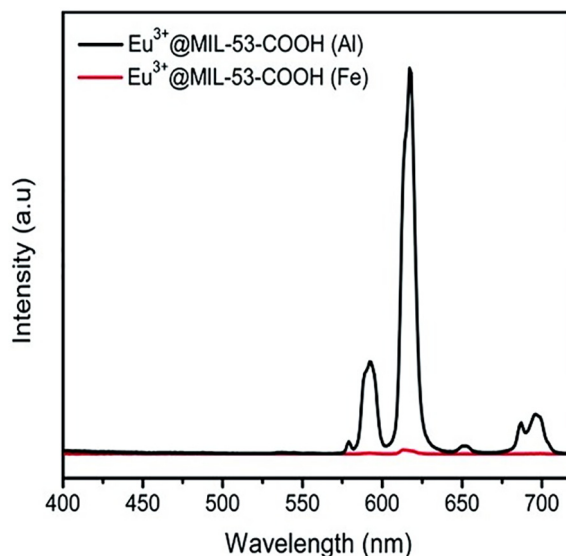

Fig. 10. Strategies for synthesizing Cr-MOFs from Fe-MOFs by metal ion exchange. (a) Reductive labilization–metathesis (Route A) and direct metal metathesis in DMF (Route B). (b) Solvent-assisted metal metathesis in acetone under milder conditions developed. Reprinted with permission from Ref. [89].

Fig. 11. Emission spectra ($λ_{ex}$ = 324 nm) of **Eu³⁺@MIL-53(Al)** and **Eu³⁺@MIL-53 (Fe)**. Adapted with permission from Ref. [94].

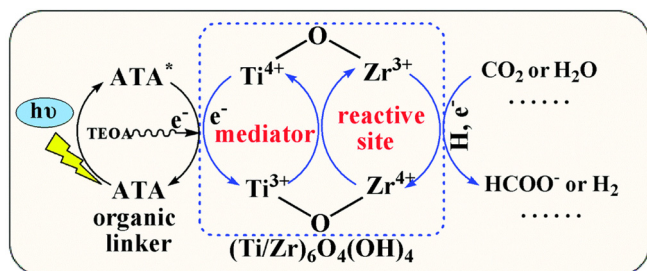**Fig. 12.** Proposed enhanced mechanism for the photocatalytic reactions over **NH₂-Uio-66(Zr/Ti)**. Reprinted with permission from Ref. [99].

enhanced photocatalytic activity was attributed to not only the increased CO_2 adsorption capability, but also other factors related to the incorporated Ti(IV) ions. The DFT calculation and electron spin resonance (ESR) results revealed that Ti(IV) center in the **NH₂-Uio-66(Zr/Ti)** acted as a mediator capable of improving the charge transfer from excited organic ligand (2-aminoterephthalate) to Zr-O clusters. The mechanism for the photocatalytic reactions is showed in Fig. 12, the Ti^{4+} centers receive electrons to form oxo-bridged Ti^{3+}-O-Zr^{4+} moieties who act as an electron donor that donates electrons to Zr^{4+} to form Ti^{4+}-O-Zr^{3+} active sites for the photocatalytic CO_2 reduction reaction (Fig. 12).

3.3. Metal ion exchange from low- to high-valence

As mentioned above, MOFs constructed with high-valence metal centers are usually more stable. So it is a feasible method to exchange low-valent metal ions in MOFs with high-valent ones to improve their stability. However, the direct metal metathesis between M(II) (divalent metal ions) and M(III) (trivalent metal ions) is commonly not feasible due to the low exchange rates and additional damage of the integrity of the MOFs. The post-synthetic metathesis and oxidation of the divalent metal ions of MOFs step by step is an alternative way to construct trivalent metal ions based MOFs. Two robust MOFs, **PCN-426-Fe(III)** and **PCN-426-Cr(III)**, were synthesized by Zhou's group via post-synthetic metathesis and oxidation of **PCN-426-Mg(II)** [100]. The related process is showed as Fig. 13. First, the Mg(II) ions of **PCN-426-Mg(II)** were exchanged with Fe(II) or Cr(II) ions to form the Fe(II)- or Cr(II)-MOFs, respectively. Then, the exchanged samples were suspended in DMF and the suspensions were bubbled with an air stream for 15 min, causing an apparent color change of the crystals from brown to dark brown, brown to dark blue, respectively. Stability tests including N_2 adsorption and PXRD measurements showed that the resulting M(III)-MOFs exhibited higher stability than the Mg(II)-MOF. The example demonstrates that

robust MOFs containing high valence metal centers can be obtained by the metal ion exchange with those with lower valence and further oxidation process.

4. Exchange reactions of ligands

The ligands are important for the construction of MOFs with desired structures and properties due to their various geometry, connectivity and functionality [21]. The pore structure and inner wall of MOFs can be tuned based on the ligand exchange reactions [23]. Furthermore, application performances of these MOFs could be optimized by these structural tuning introduced by ligand exchange reactions. Herein, the ligand exchange reactions are classified and discussed in detail according to the coordinating groups of the ligands.

4.1. Bridging pyridine ligand exchange

Pyridine ligands are usually used as pillars to connect layers in MOFs with pillared-layered structures. These pyridine pillars can be exchanged by those with different length or functional groups, which can cause changes in MOF sructures and properties.

The pore sizes of MOFs can be adjusted when the pyridine ligands in MOFs are exchanged by those with different length. For example, Bharadwaj's group synthesized a twofold interpenetrated pillared-bilayer framework, {[Zn₃(TCBPA)₂(BPyE)(DMF)]·(1 8DMF)(6H₂O)}ₙ (**75**), and studied its pillar linker substitution reactions with different dipyridyl linkers of different lengths as showed in Fig. 14a [101]. The crystals of **75** were immersed in DMF solutions of AZP, PyINA, and BiPy at room temperature for 65, 70, and 50 h, resulting in {[Zn₃(TCBPA)₂(AZP)(DMF)]·(12DMF)(6H₂O)}ₙ (**76**), {[Zn₃(TCBPA)₂(PyINA)(DMF)]·(12DMF)(4H₂O)}ₙ (**77**), and {[Zn₃(TCBPA)₂(BiPy)(DMF)]·(10DMF)(5H₂O)}ₙ (**78**), respectively (Fig. 14b). Obviously, the pore sizes and pore surfaces in these four MOFs were different, because the pillar linkers, BPyE, AZP, PyINA, and BiPy, have different lengths and functional groups. The shortest pillar linker (PZ and DABCO) and the longest one (DPyB) tested in this study could not substitute any other linker in the aforementioned MOFs, but a DPyB based MOF, {[Zn₃(TCBPA)₂(DPyB)(H₂O)]·(20DMF)(4H₂O)}ₙ (**79**), was directly synthesized and it was used to the ligand exchange reaction with a shorter linker AZP. Surprisingly, structural analysis revealed that a linker exchange reaction occurred and a new compound, {[Zn₃(TCBPA)₂(AZP)(DPyB)₀.₅]·(15DMF)(3H₂O)}ₙ (**80**), was obtained (Fig. 14c). All of these reactions took place in a SC-SC manner and were monitored directly through X-ray crystallography. The distance between two connecting SBUs, the coordination geometry, coordination environment of middle Zn(II) center in the SBU,
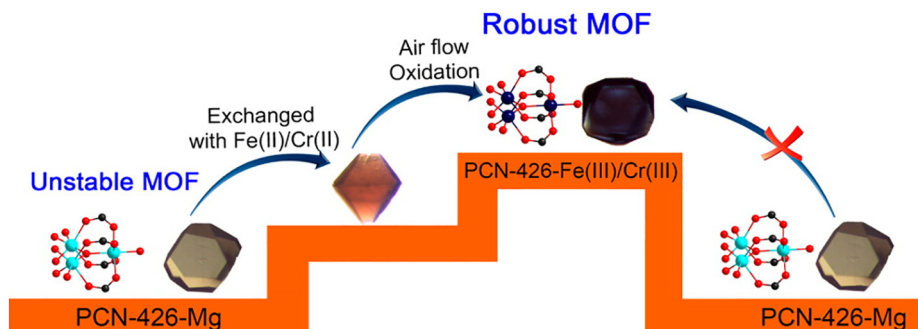

Fig. 13. The synthetic route from unstable **PCN-426-Mg(II)** to robust **PCN-426-Fe(II)/Cr(II)** after metathesis, then to **PCN-426-Fe(III)/Cr(III)** after metal node oxidation. Reprinted with permission from Ref. [100].
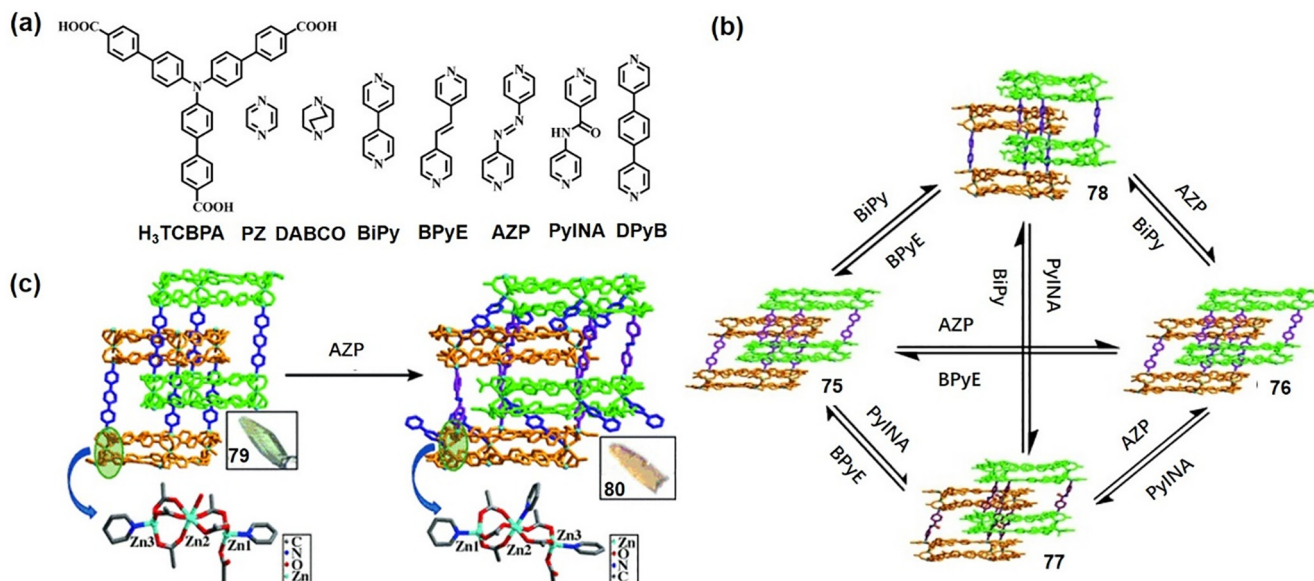
Fig. 14. (a) Ligand H_3TCBPA and different ditopic pillar linkers used for the SC-SC, (b) Summary of the linker exchange reactions among {[Zn_3(TCBPA)$_2$(BPyE)(DMF)]·(18DMF)(6H_2O)}$_n$ (**75**) and its pillar linker exchange products **76–78**, (c) Figure illustrating the SBU cross-linking during the conversion of {[Zn_3(TCBPA)$_2$(DPyB)(H_2O)]·(20DMF)(4H_2O)}$_n$ (**79**) to {[Zn_3(TCBPA)$_2$(AZP)(DPyB)$_{0.5}$]·(15DMF)(3H_2O)}$_n$ (**80**). Adapted with permission from Ref. [101].

and the orientation of the coordinated solvent molecule played important roles in this unique linker exchange reaction.

The exchange of pyridine ligand using another shorter one can lead to the partial reorganization of the MOF framework structure. Shin and co-workers reported a post-synthetic exchange of the organic linkers, accompanied by a 2D reorganization of the three-periodic framework (Fig. 15) [29]. The dark cyan crystals of as-synthesized [Ni_3(BTC)$_2$(BiPy)$_3$(H_2O)$_2$]·xDMF (**81**) were soaked in a DMF solution of pyrazine (PZ) at 100 °C for 1–2 weeks to form greenish cyan [Ni_3(BTC)$_2$(PZ)$_3$(H_2O)$_2$] (**82**) via the exchange of the neutral diptotic pillars. Single crystal analyses revealed that the space group of **82** was the same as that of original MOF, but the lattice parameters of new MOF were significantly different from original MOF. The pillar exchange led to the compressed stacking of the two-periodic sheets of a **bex** topology and the 2-D structural reorganization, with the increasing of rigidity in the framework. However, the reduction of the pore volume and the surface area was caused by the shortening of pillar length, which was con-

firmed by the reducing of BET surface area from 1510 to 1060 m^2 g^{-1}. A completely different structure of [Ni_6(BTC)$_4$(PZ)$_{4.75}$(H_2O)$_5$] was obtained by the removal of half of the PZ pillars interconnecting the mononuclear Ni centers along the crystallographic b-axis in **82** (one-sixth of the total PZ linkers). It was believed that the stable one-periodic rhomboidal chain as a SBB played a pivotal role during these transformations. These experiment results indicate that the bridging pyridine ligand exchange with those of different lengths can tune the MOF structure.

Pyridine ligand exchange reaction can enhance the gas adsorption capacities and photocatalytic efficiencies of MOFs through creating structural defects. Two cases of defective MOF obtained through ligand exchange were reported by Masoomi and co-workers[102]. The as-synthesized [Zn_2(OBA)$_2$(4-BPDB)]$_n$·(DMF)$_2$ (**TMU-4**, **83**) and [Zn(OBA)(4-BPMB)$_{0.5}$]$_n$·(DMF)$_{1.5}$ (**TMU-6**, **85**) were placed in the DMF solutions containing 4-BPMB and 4-BPDB at 120 or 80 °C for 21 days or 24 h to obtain **TMU-6′** (**84**) and **TMU-4′** (**86**), respectively. The SEM images of these
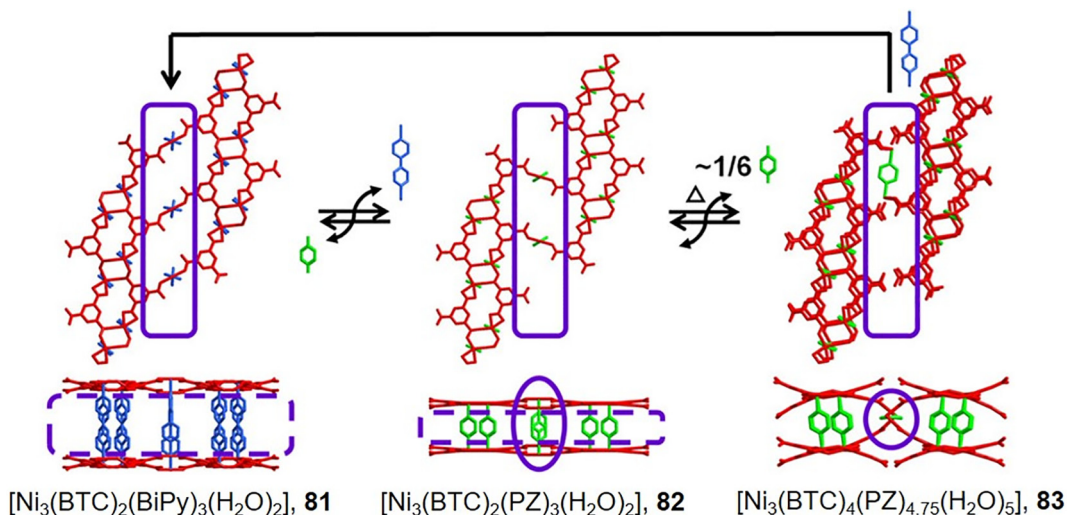

$[Ni_3(BTC)_2(BiPy)_3(H_2O)_2]$, **81** $[Ni_3(BTC)_2(PZ)_3(H_2O)_2]$, **82** $[Ni_3(BTC)_4(PZ)_{4.75}(H_2O)_5]$, **83**

Fig. 15. A scheme of reversible SCSC transformations by ligand exchange, deletion, and insertion. Adapted with permission from Ref. [29].
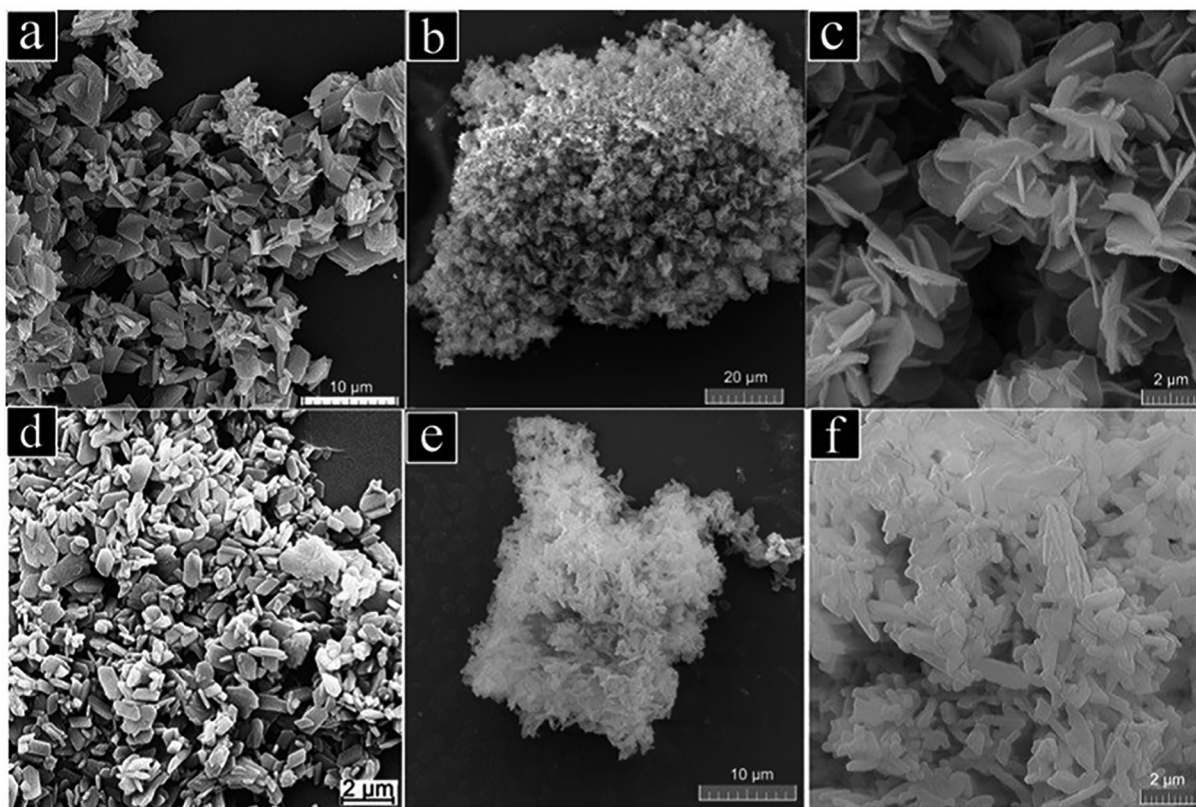
Fig. 16. FE-SEM images of (a) parent **TMU-4**, (b) **TMU-4′** synthesized via ligand exchange, (c) magnification image of **TMU-4′**, (d) parent **TMU-6**, (e) **TMU-6′** synthesized via ligand exchange and (f) magnification image of **TMU-6′**. Reprinted with permission from Ref. [102].

compounds revealed they have similar morphologies (Fig. 16). N_2 sorption measurements revealed that **TMU-4** and −**6** were nonporous but **TMU-4′** and **TMU-6′** were porous with BET surface areas of 207 and 68 m^2 g^{-1}, respectively. The increase in the BET surface area was attributed to the introduced structural defects (unsaturated metal sites or ligand missing defects) during the process of ligand exchange. In addition, it was also demonstrated that the structural defects (unsaturated metal sites) created by ligand exchange also could enhance the photocatalytic activity of **TMU-4′** and −**6′** for Cr(VI) reduction attributing to the improvement of Cr(VI) adsorption capacity.

It is well-known that the magnetic track of MOF materials is mainly composed of the combination of ligand orbits and metal ion orbits (t_{2g} and e_g), orbital overlapping can cause the antiferromagnetic coupling effect, and the orthogonality of the orbits is easy to cause the ferromagnetic coupling effect [103]. The ligand exchange reactions involve the breaking and reforming of chemical

bonds, which caused subtle geometry changes of coordination environment of metal centers. These subtle changes could modify the magnetic properties of MOFs without topological change. Shao and co-workers selected a water-stable MOF, {[Ni$_{1.5}$(ABTC)(AZP)(H$_2$O)$_2$]·6·.5H$_2$O}n (**87**), as the template to generate {[Ni$_{1.5}$(ABTC)(BiPy)(H$_2$O)]·6H$_2$O}$_n$ (**88**), {[Ni$_{1.5}$(ABTC)(BPE)(H$_2$O)]·8·.5H$_2$O}$_n$ (**89**) and {[Ni$_{1.5}$(ABTC)(NH$_2$-BiPy)-(H$_2$O)]·7·.5H$_2$O}$_n$ (**90**) through ligand exchange reactions in H$_2$O/CH$_3$CN mixture at 80 ℃ for 2, 4, and 10 days, respectively [77]. The appearance of core–shell crystals during the exchange process showed that the exchange reaction occurred from the decomposition to depth of **87**. As shown in Fig. 17a, the structures of these phases obtained through ligand exchanged were similar to the pristine MOF, and only the ligand AZP was replaced by BiPy, BPE and NH$_2$-BiPy, respectively. Magnetic studies showed that **88** and **89** showed different behavior from **87**. Compared with that of **87**, the ferromagnetic-like behavior of **88** was strengthened at low temperature due to the orthog-
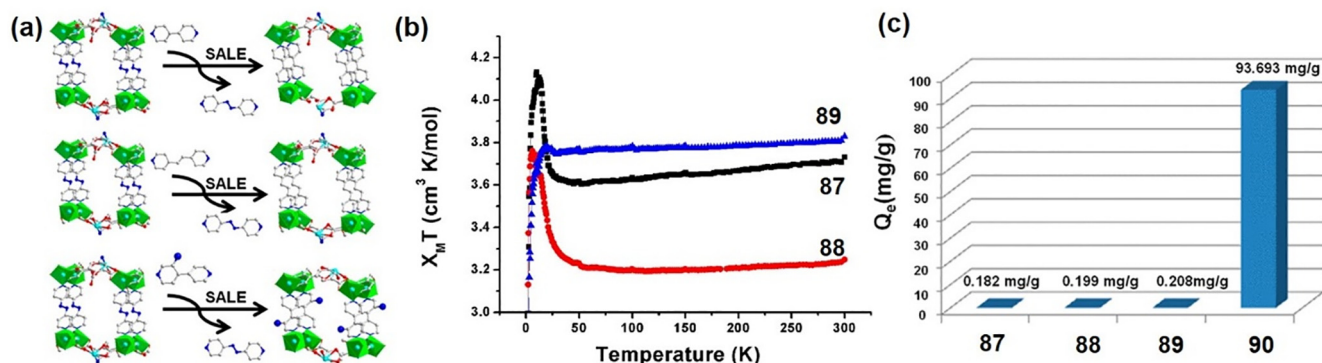

Fig. 17. (a) Changes in structure before and after exchange reaction. (b) Temperature dependence of χ_MT for {[Ni$_{1.5}$(ABTC)(AZP)(H$_2$O)$_2$]·6·.5H$_2$O}n (**87**) and its ligand exchange products **88**–**89**. (c) Adsorption properties of **87**–**90** for Hg^{2+} in water. Adapted with permission from Ref. [77].

onality of magnetism orbit resulted from the reduction of dihedral angle between Ni^{2+} and the connected carboxyl group. In contrast, the enhanced antiferromagnetic was observed in **89** due to the further orbit overlap by the increase of the dihedral angles (Fig. 17b). In addition, Hg^{2+} adsorption experiments were carried out to study the adsorptive removal ability of **87** and **90**. Compared with **87** (0.182 mg/g), **90** showed a significantly higher ability to remove Hg^{2+} with an adsorption capacity of 93.693 mg/g after 5 h, which was attributed to the strong binding interactions between Hg^{2+} and its $-NH_2$ groups on pore surface (Fig. 17c).

Pyridine ligand exchange can also serve as a strategy of introducing special groups with adsorptive and catalytic activity into the MOF framework. $[Cu_3(TPTC)_2(2-NH_2-PZ)(H_2O)]\cdot12DMF$ (**92**), which is not available by direct synthesis, were synthesized by Wang and co-workers through the exchange reaction of $[Cu_3(TPTC)_2(PZ)(H_2O)]$ (**91**) with 2-NH_2-pyz in the SC-SC manner [46]. SCXRD analysis showed that **92** maintained the overall frame-work of the parent MOF, but there were free amino groups on the pore surface. Compared with **91**, **92** not only showed a larger adsorption enthalpy for CO_2 due to the strong interaction between functional $-NH_2$ groups and CO_2 molecules but also a high catalytic performance for the Knoevenagel condensation reactions of various aldehydes (including electron-donating and electron-withdrawing aromatic aldehydes) with ethyl cyanoacetate (Fig. 18).

Flexible MOFs are a class of promising adsorbents for gas separation with high adsorption selectivity and high working capacity [9,104], due to their tunable pore aperture and pore volume by the response to external stimuli [105]. However, the number of flexible MOFs is smaller than that of rigid MOFs, because constructing flexible MOFs is sometimes difficult by the direct synthetic method. Pyridine ligand exchange can serve as a versatile strategy of preparing flexible MOFs by replacing rigid ligands with flexible or semi-flexible ligands. He and co-workers reported the
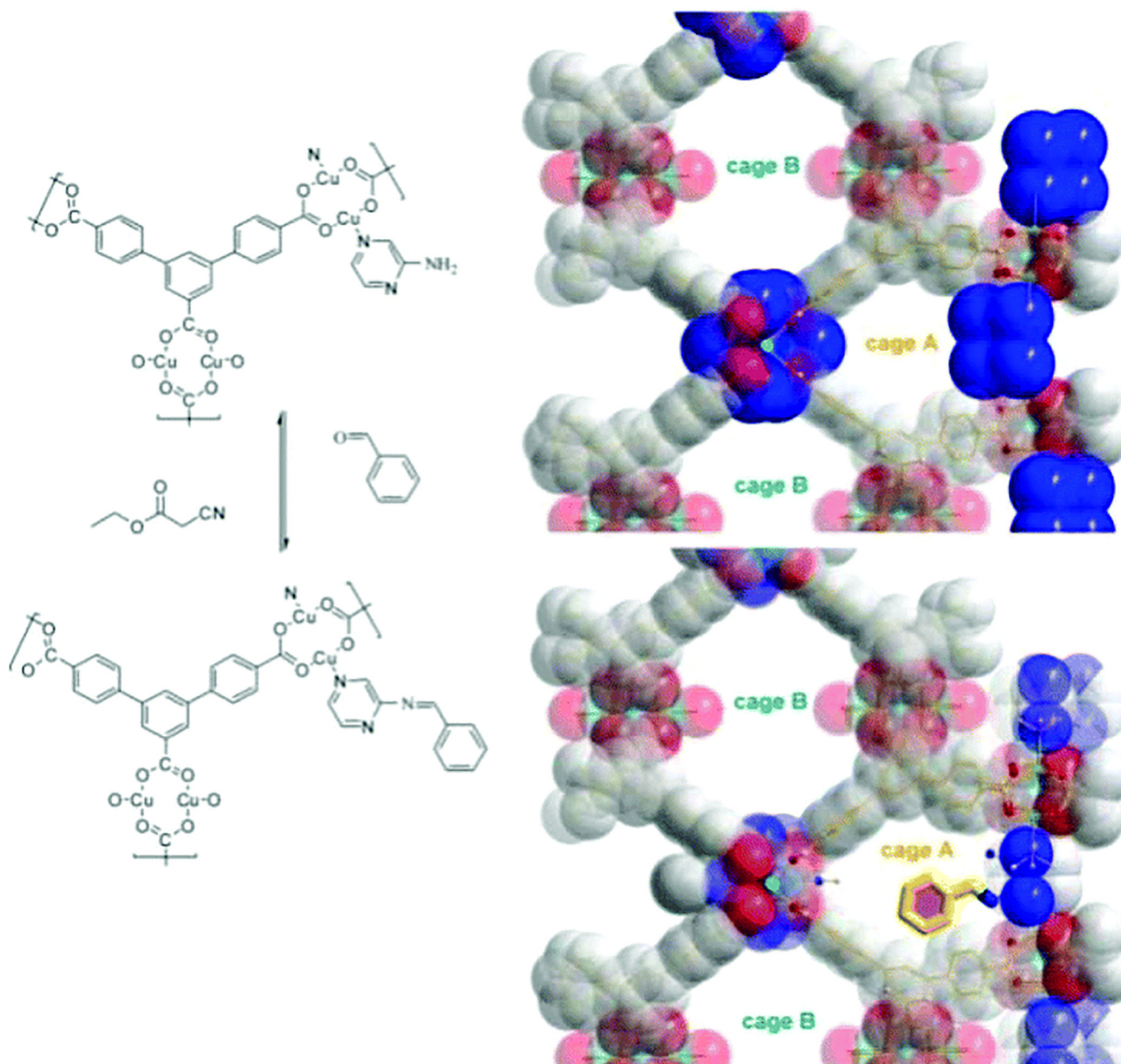

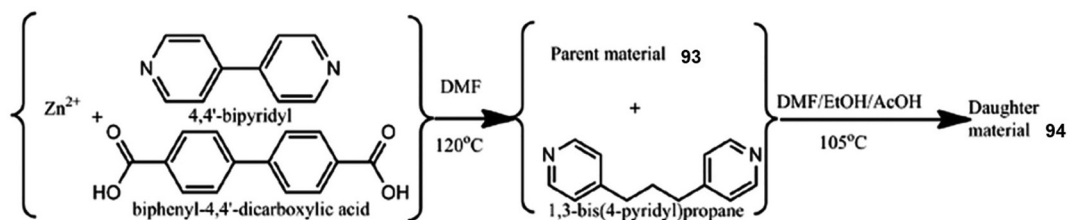**Fig. 18.** Schematic representation of the Knoevenagel reaction in the MOFs. Reprinted with permission from Ref. [46].

Fig. 19. Synthesis route of parent Zn$_8$(BPDC)$_8$(BiPy)$_8$ (**93**) and daughter Zn$_8$(BPDC)$_8$(BPP)$_8$ (**94**) samples. Reprinted with permission from Ref. [25].
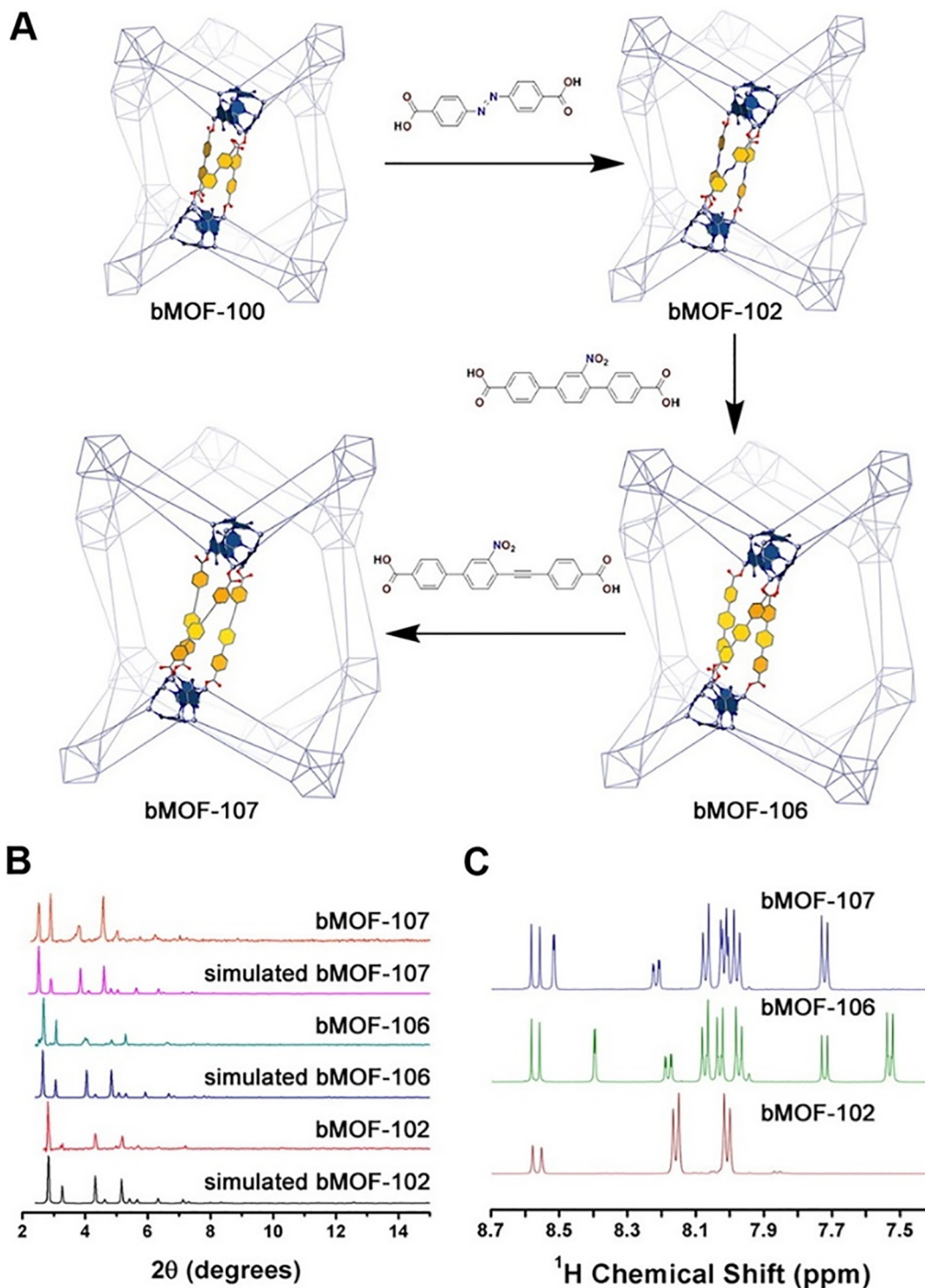

Fig. 20. Schematic representation of sequential pore expansion from **bMOF-100** to **bMOF-102** to **bMOF-106** to **bMOF-107** via ligand exchange. Reprinted with permission from Ref. [59].

conversion of a 3D rigid MOF (**93**) constructed by trinuclear Zn(II) clusters interconnected by BPDC^{2-} bridging linkers and BiPy pillars into Zn$_8$(BPDC)$_8$(BPP)$_8$ (**94**) with a novel 2D flexible network through ligand exchange (Fig. 19) [25]. The flexible 2D MOF could not be obtained by direct synthesis. The ligand exchange reaction was completed by soaking **93** into a concentrated fresh DMF/EtOH/MeCOOH (v:v:v = 4:1:0.1) solution of BPP at 105 ℃ without stirring for four consecutive 3d exchanges. The authors believed that acetic acid played an important role in the ligand exchange process, as it promoted the disassembly of the parent metal cluster through replacing carboxylate oxygens and coordinating to the Zn(II) ions. Then BPDC^{2-} replaced the acetate and BPP replaced BiPy to form a new topology completely different with the original one. The CO$_2$ and N$_2$ adsorption measurements of **93** and **94** were carried out. Different from the parent MOF, the CO$_2$ sorption isotherms of **94** at different temperatures were the typical isotherms for flexible MOFs (with adsorption steps and large hysteresis), which indicated structural flexibility and crystal phase transition upon CO$_2$ sorption attributing to the strong interaction between the MOF framework and guest CO$_2$ molecules with large quadrupole moment. In contrast, N$_2$ adsorption capacity of **94** was negligible due to the weak adsorbate-adsorbent interactions, leading to a high CO$_2$/N$_2$ adsorption selectivity (80 at 1 bar and 273 K).

4.2. Bridging carboxylate ligand exchange

Carboxylate ligands as bridging linkers in MOFs are various [7], including monodentate, bidentate and polydentate ones. They can be exchanged by the similar ones with different length and functional groups to adjust the pore structures and properties of MOFs.

Two or even more different ligands can be introduced into a MOF via sequential ligand exchange reactions to increase their diversity and complexity in composition and functionality. Liu and co-workers studied the pore expansion process based on the ligand exchange of **bMOF-100** (**95**) [59]. The crystals of **bMOF-100** (Zn$_8$(AD)$_4$(BPDC)$_6$O$_2$·(cation)$_4$, cation = dimethylammonium) were converted to **bMOF-102** (**96**) crystals via exchanging the BPDC^{2-} ligands with AZDC^{2-}; then the as-produced **bMOF-102** crystals were converted to **bMOF-106** (**97**) crystals through exchange of AZDC^{2-} with NO$_2$-TPDC^{2-}; and finally the as-produced **bMOF-106** crystals were converted to **bMOF-107** (**98**) through exchange of NO$_2$-TPDC^{2-} with NO$_2$-ePTDC^{2-}. The series of exchange reactions were carried out at 75 ℃ with DMF as solvent (Fig. 20). These exchange reactions occurred from the crystal periphery to the crystal core, which was confirmed by real-time monitoring of the conversion processes from **bMOF-100** to **bMOF-102** and from **bMOF-102** to **bMOF-106**, indicating that the postsynthetic ligand exchange could be used to create structurally

heterogeneous MOF crystals (intermediate product MOFs) with internal directional porosity gradients by terminating the exchange reaction prior to complete crystal conversion. In a word, the incomplete transformation of each step makes the final exchanged MOF have complex pore structure. Similarly, multiple functional moieties can be introduced into the same framework to prepare multifunctionalized MOFs. Rosi's group installed three functional groups (–NH$_2$, –N$_3$, and -F) into **bMOF-100** through stepwise BPDC^{2-} ligand exchange with other ligands of similar lengths, NH$_2$-BPDC^{2-}, N$_3$-BPDC^{2-}, and F-BPDC^{2-} [61]. The ratios of the three functional groups in the MOF pores were tunable by controlling the reaction time of every step. These functionalized crystals resulted from ligand exchange could be modified with large dye and quencher molecules to explore the distribution of functional moieties within the MOF. Spectrophotometric analysis of the dye-quencher MOFs suggests a random distribution of functional groups in binary functionalized **bMOF-100**. These examples indicated that ligand exchange reactions can realize the rational control of pore sizes and environments in MOFs.

Some of the carboxylate ligand exchange reactions could bring about topological changes of MOFs. For example, ***lcs***-bio-MOF-100 (**1 0 0**) with twist-boat pore was prepared by Miera and co-workers based on the exchange reaction of the pristine ***dia-c*** phase (**99**) with chair pore [60]. The exchange reaction was carried out by soaking the parent samples into the DMF solution of H$_2$IrL at room temperature over 24 h to perform the BPDC^{2-} ligand exchange with IrL^{2-} (Fig. 21). This work shows that MOFs can undergo architectural modifications via ligand exchange.

With more and more research on defective MOFs, ligand exchange in defective **UiO-66** was investigated by Taddei and co-workers [106]. The possible outcomes of exchange reactions of a terephthalic acid analogue on **UiO-66** are shown in Fig. 22. The exchange of monocarboxylic acids grafted at defective sites always preferentially occurred regardless of temperature and solvent when the defective **UiO-66** was soaked in a solution of a terephthalic acid analogue, which was demonstrated by a 1:1 ratio between the incoming linker and the modulator in situ solution. Meanwhile, the ratio of 1:1 but not 1:2 provided evidence that the defects had missing-cluster but not missing-ligand nature (Fig. 22e). The monocarboxylic ligand exchange in defective sites with ditopic carboxylic acid ligand can affect the properties of MOFs by decreasing the porosity and leaving the second carboxylate uncoordinated and exposed in the pores. In other words, ligand exchange is an alternative way to regulate the porosity and pore environment of defective MOFs.

Ligand exchange could introduce functional groups into the targeted MOFs and adjust their application performances [23]. In order to remove harmful ions from water, specific functional groups with strong interaction with harmful ions can be intro-
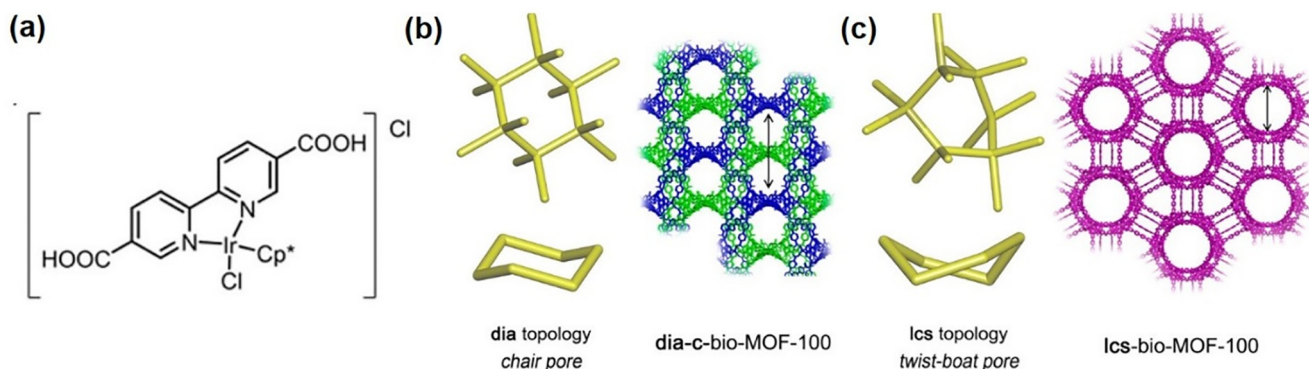

Fig. 21. (a) Representation of H$_2$IrL. (b) Interpenetrated ***dia-c*** form with a chair conformation of the hexagonal pores and (c) ***lcs*** form showing the twist-boat conformation of the hexagonal pores. Adapted with permission from Ref. [60].
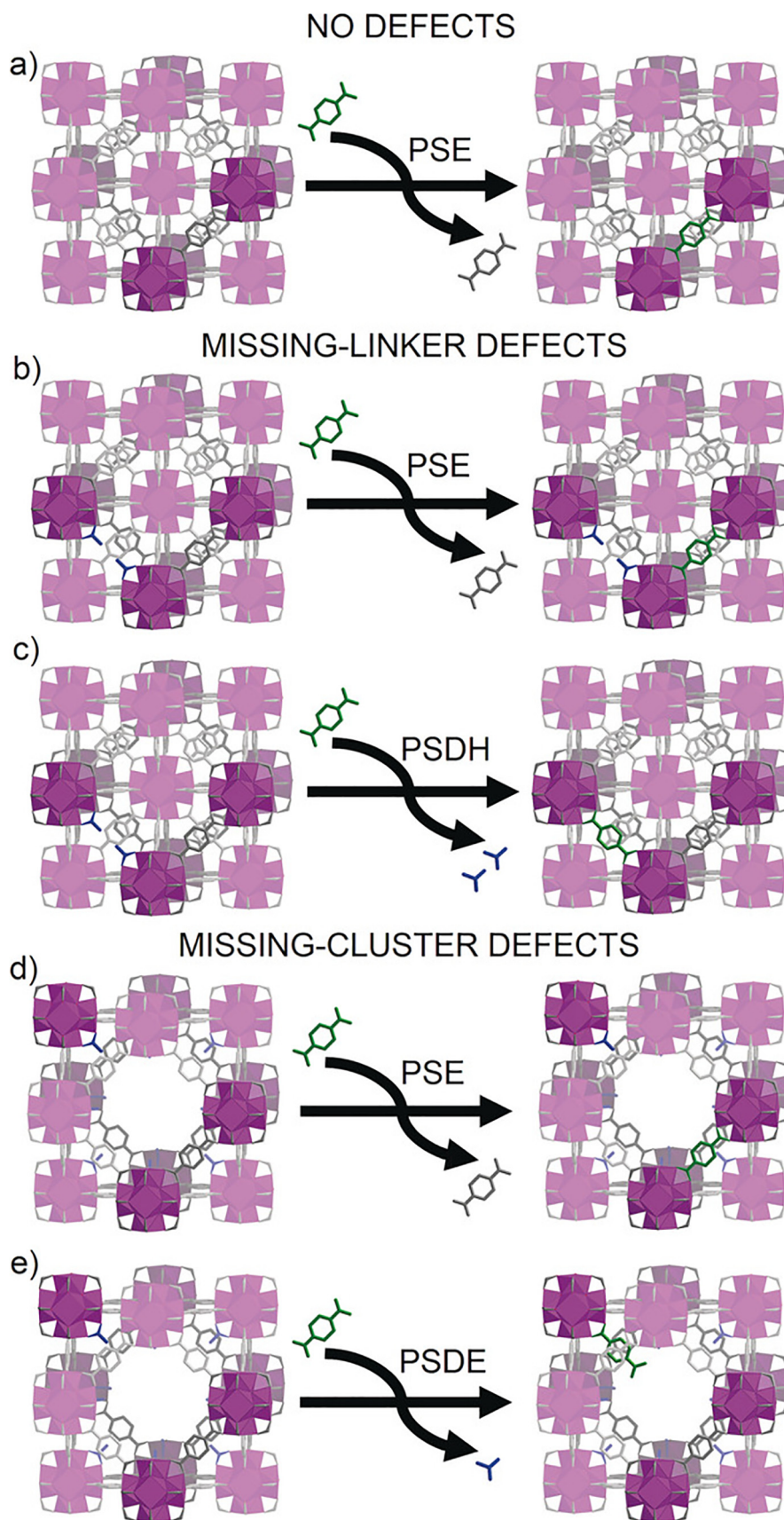
Fig. 22. Possible outcomes of exchange reactions of a terephthalic acid analogue (green) on **UiO-66** (PSE: post-synthetic ligand exchange; PSDH: post-synthetic defect healing; PSDE: post-synthetic defect exchange). Reprinted with permission from Ref. [106].

duced into MOFs through carboxylate ligand exchange. Hu and co-workers reported a Zr-MOF (**MFC-S**, **102**) functionalized by mercapto (–SH) groups and used for the Hg^{2+} removal from water [44]. **MFC-S** could not be directly synthesized but obtained through ligand exchange by immersing the pristine **MFC-O** sample into the mercaptoacetic acid solution at 60 ℃ for 24 h with an exchange ratio of 14% (Fig. 23a). Compared with **MFC-O**, **MFC-S** exhibited obvious improvement of Hg^{2+} adsorption capacity due to the introduced –SH groups on pore surface. A good selectivity and reusability make the **MFC-S** potential in the removal mercury ions from water (Fig. 23b).

In addition, special groups can be introduced into MOFs to stabilize the inserted active metal sites, avoid agglomeration of active metal particles and enhance their catalytic activity by carboxylate ligand exchange reactions. A thiocatechol-functionalized **UiO-66** (**1 0 3**) material, **UiO-66-TCAT** (**1 0 4**), was synthesized by Fei and co-workers through postsynthetic ligand exchange and metallized with Pd to form **UiO-66-PdTCAT** (Fig. 24a) [47]. The catalytic activities of **UiO-66**, **UiO-66-TCAT**, and **UiO-66-PdTCAT** in the reactions of oxidizing sp^2 C – H bond to C – O or C – X (X = Cl, Br, I) bond were studied. The results showed that **UiO-66-PdTCAT** exhibited the highest catalytic performance, which resulted from the introduction of Pd centers as the catalytic active sites into a sulfhydryl functionalized MOF (Fig. 24b). Clearly, ligand exchange is a facile and mild functionalization approach to synthesize a robust **UiO-66** material with a sulfur-containing thiocatechol sites to load accessible and unsaturated mono(thiocatecholato) metal centers for enhancing catalytic activity.

Some reactive functional groups can be also introduced into MOFs through carboxylic acid ligand exchange to realize some special chemical reactions in MOFs. For example, **NU-125-HBTC** (**1 0 6**) with free carboxylic acid (–COOH) groups was synthesized by Farha's group through ligand exchange reaction by soaking **NU-125-IPA** (**1 0 5**) in DMF solution of H_3BTC at 80 °C overnight [107]. The successful exchange of IPA^{2-} with $HBTC^{2-}$ and the introduction of –COOH groups on the MOF pore surface was confirmed by diffuse reflectance infrared Fourier-transformed spectroscopy (DRIFTS). The free –COOH groups were utilized for the selective monoesterification of trimesic acid. Similarly, the azide or acetylene group functionalized **UiO-67** (**1 0 7**) was synthesized by Fluch and co-workers through a linker exchange of original $BPDC^{2-}$ ligand with $BPDC-N_3^{-}$ or $BPDC-C≡C^{2-}$ [108]. The ligand exchange reaction was performed by stirring **UiO-67** and $H_2BPDC-N_3$ or $H_2BPDC-C≡C$ in a mixture solvent (THF:MeOH:H_2O, v:v: v = 3:2:1) at room temperature for 24 h. Then the resultant MOFs,

108 and **109**, were subjected to the click reactions with 1-ethynyl-4-(trifluoromethyl)benzene and 4-azido-1,1,1-trifluorobutane in the presence of copper catalyst, respectively, producing functional MOFs with "clicked" triazole groups and reduced pore sizes. This example provided a powerful method of introducing orthogonal modifications into known MOF architectures. In addition, the MOFs with covalent anchors introduced via ligand exchange can provide a platform to perform click reactions with the fluorophores. Zhou's group reported a related example [48]. First, a variety of functional groups were incorporated into **PCN-333-Fe** or **-Sc** by using various BTB^{3-} derivatives ($OH-BTB^{3-}$, NH_2-BTB^{3-}, azide-BTB^{3-}, alkene-BTB^{3-}, alkyne-BTB^{3-} and chiral-BTB^{3-}) with different substituents at the 2-position of the central benzene ring to exchange the original ligands BTB^{3-} of **PCN-333**. Then, the azide-functionalized **PCN-333-Sc** was used for the click reaction of the MOF with alkyne-BODIPY (BODIPY = 4,4-difluoro-4-bora-3a,4a-diaza-s-indaene) in THF under the presence of the catalyst CuI. It was found that the resultant BODIPY-clicked **PCN-333-Sc** showed a strong fluorescence in both suspension and solid-state status (Fig. 25).

4.3. Bridging azole ligand exchange

Although many MOFs constructed by metal centers and azole ligands (especially imidazoles and pyrazoles) show higher stability [109], imidazole-to-imidazole and imidazole-to-triazole ligand exchange reactions have been reported for this type of MOFs [32,43]. Similar to the ligand exchange reactions mentioned in 4.1 and 4.2, the azole ligand exchange also can be used to modify the structure and property of desired MOFs.

Adsorption performances could be modified by introducing functional groups that could enhance the interactions between MOFs and target guest molecules. Tsai and co-workers performed such a study based on **ZIF-8** (also known as **MAF-4**, **110**). The n-butanol, methanol, methanol, and methanol suspensions of **ZIF-8** were added into an n-butanol solution of SHBzIm, a methanol solution of NH_2BzIm, an n-butanol solution of PhIm, and a 1:1 methanol/DMF solution of NO_2Im, respectively. The obtained mixtures were heated at 100, 60, 60, and 60 ℃ for 72, 168, 168, and 168 h to obtain mixed-linker products (LeZIF8-SHBzIm$_{72h}$, **111**; LeZIF8-NH_2BzIm_{168h}, **112**; LeZIF8-PhIm$_{168h}$ **113**; LeZIF8-NO_2Im_{168h}, **114**), respectively (Fig. 26a) [32]. Compared with ZIF-8 (1605 m^2 g^{-1}), The BET surface area based on N_2 adsorption at 77 K of these linker exchanged products (**111**, 1416 m^2 g^{-1}; **112**,1108 m^2 g^{-1}; and **113**, 1579 m^2 g^{-1}) with the same SOD topology did not change significantly except **114** (633 m^2 g^{-1}) in which the ***frl*** topology structure

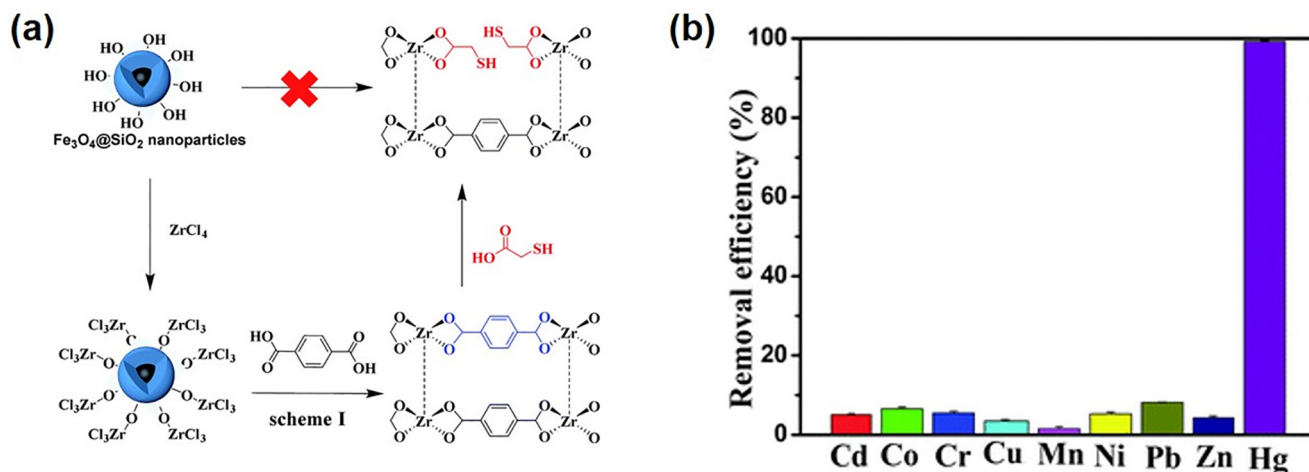**Fig. 23.** (a) Schematic diagram of the preparation of **MFC-S**. (b)Selectivity of **MFC-S** for Hg^{2+}. Adapted with permission from Ref. [44].
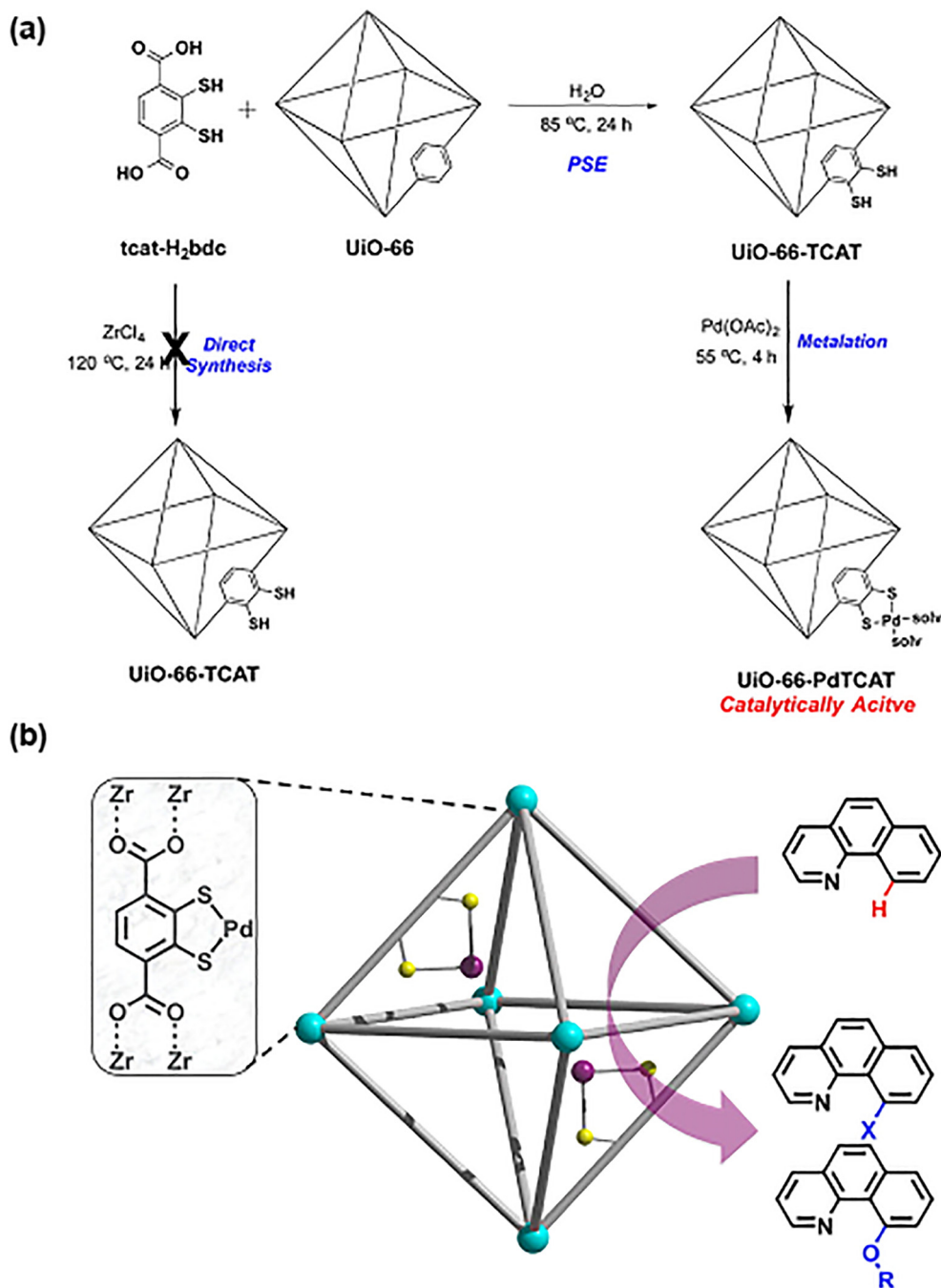
Fig. 24. (a) Synthesis of **UiO-66-TCAT** and **UiO-66-PdTCAT**; (b) the catalytic activities of **UiO-66-PdTCAT**. Adapted with permission from Ref. [47].

was dominant over the SOD topology structure. However, compared with that for **ZIF-8** (33.8 cm^3 g^{-1}), the quantities of CO_2 adsorbed at 273 K and 900 mmHg for **111** (77.21 cm^3 g^{-1}) and **114** (76.02 cm^3 g^{-1}) were doubled to ~77 cm^3 g^{-1} (Fig. 26b). The improved CO_2 adsorption capacities of **111** and **114** were attributed to the –NO$_2$ pulling electron density away from the hydrogen atoms on the linkers or the –SH pulling electron away from the hydrogen bound to sulphur. In addition, compared with **111**, **114** has a higher uptake in adsorbing CO_2 without the need for high surface area attributing to the strong dipole-quadrupole interactions between CO_2 with –NO$_2$ functionalities in its structure. Hydrophilic or hydrophobic groups also can be introduced into the pores of MOFs to tune their affinities toward water molecules. The selective ligand exchanges of a series of mixed-linker zeolitic

imidazolate frameworks (ZIFs, **ZIF-69**, −**78**, and −**76**,) were reported by Lalonde and co-workers [43]. During the exchange processes, only the benzimiadazolate-containing linkers in **ZIF-69**, −**78**, and −**76** were replaced by 5-(trifluoromethyl)benzimidazole ligands to form the isostructural **SALEM-10**, **SALEM-10b**, and **SALEM-11**, respectively. Water contact angle measurements of the ZIFs and ligand-exchanged SALEM materials were carried out. SALEMs showed significantly larger contact angles than the original ZIFs, which was attributed to the introduction of trifluoromethyl groups on the pore surface through the ligand exchanges.

Ligand exchange can also serve as a way of introducing atoms with lone pair electrons to enhance the π-π and Lewis acid-base interaction between MOFs and target guest molecules. Yan and co-workers synthesized a benzotriazole-containing **ZIF** (**ZIF-7-M**)
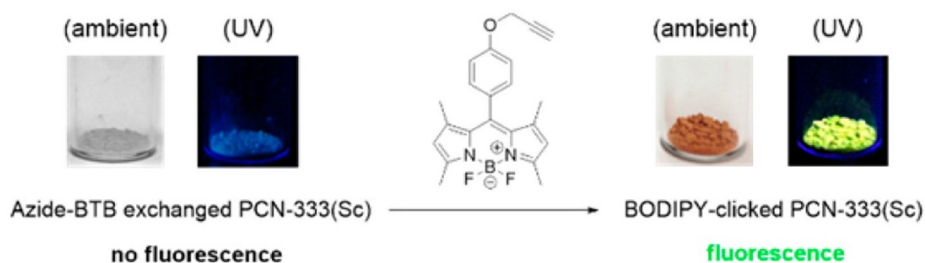
Fig. 25. Click reaction scheme performed on **PCN-333-Sc** with BODIPY fluorophore. Photographs are before and after BODIPY introduction on **PCN-333-Sc**. Adapted with permission from Ref. [48].
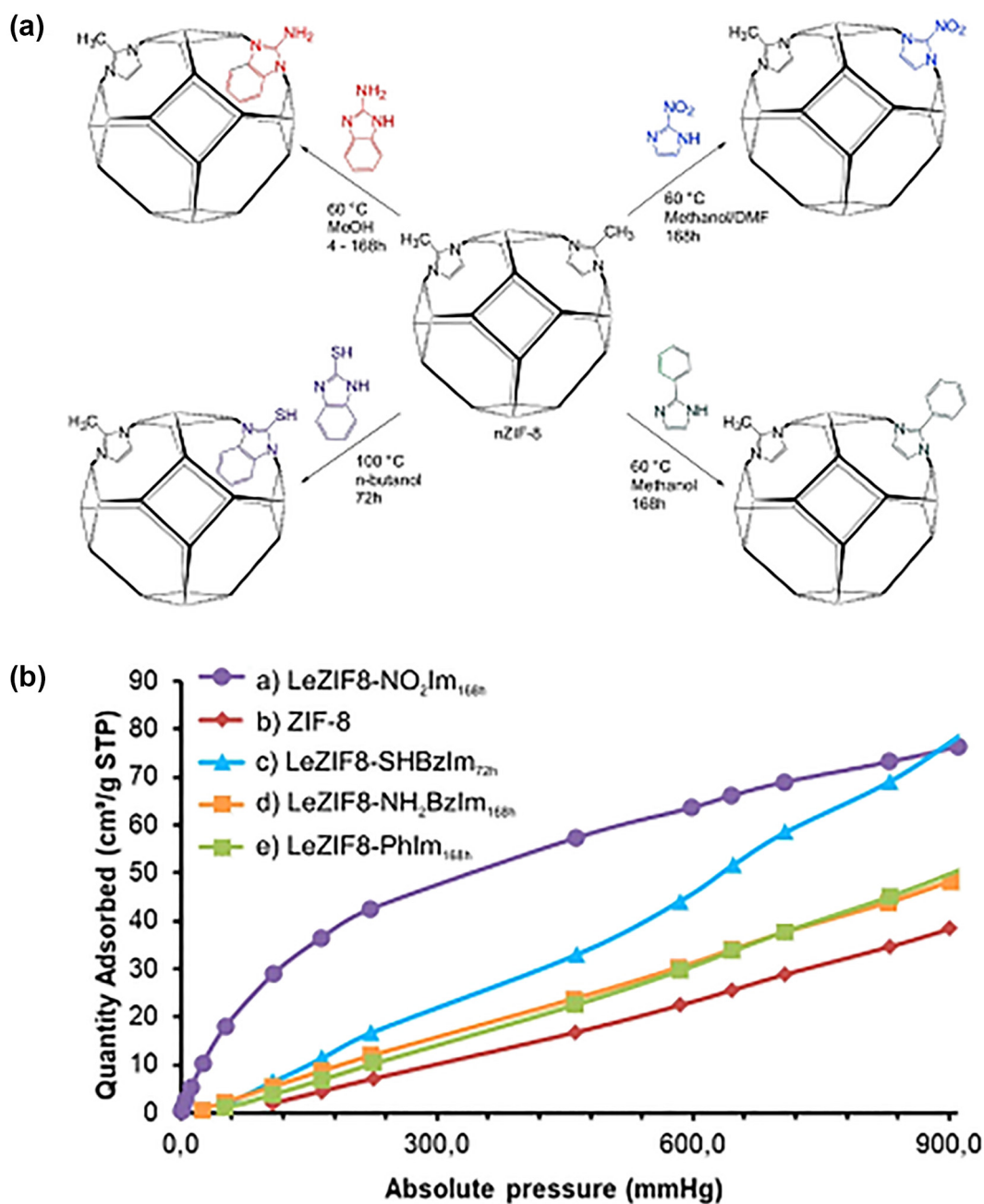

Fig. 26. (a) General scheme of ligand exchange of **ZIF-8**. (b) CO_2 isotherms obtained at 273 K of a) LeZIF8-NO$_2$Im$_{168h}$, b) ZIF-8, c) LeZIF8-SHBzIm$_{72h}$, d) LeZIF8-NH$_2$BzIm$_{168h}$ and e) LeZIF8-PhIm$_{168h}$. Adapted with permission from Ref. [32].
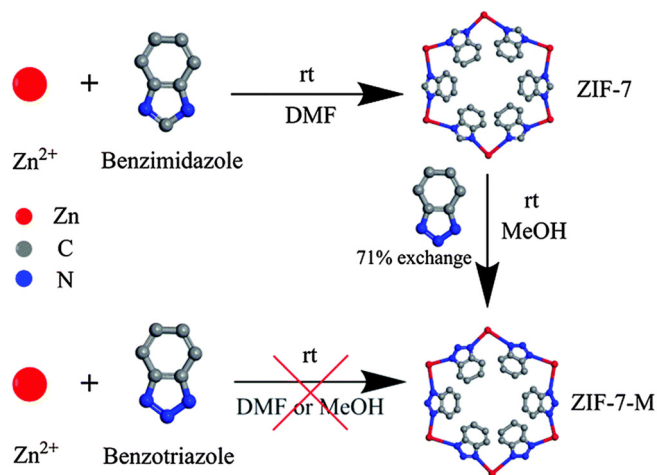
Fig. 27. Schematic demonstration for the synthesis of benzotriazole-containing ZIF with PSE strategy. Reprinted with permission from Ref. [110].

via a 71% exchange of benzimidazole in template **ZIF-7** with benzotriazole in methanol for 10 days (Fig. 27) [110]. However, the attempt to synthesize **ZIF-7-M** directly by de novo synthesis failed. As the authors mentioned, the temperature had a little effect on the ratio of the exchange reaction, but a high concentration of benzotriazole was favorable for the exchange. Compared with **ZIF-7**, **ZIF-7-M** showed a larger adsorption enthalpy for cyclohexene and benzene, but a smaller adsorption enthalpy for cyclohexane due to the introduced benzotriazole providing uncoordinated nitrogen atoms whose lone pair electrons can improve the π-π interaction between MOF framework and guest molecules with conjugated group. In addition, **ZIF-7-M** not only exhibited faster adsorption kinetics but also gave a much larger adsorption capacity for Cd^{2+} ions than **ZIF-7**, which was attributed to the induced uncoordinated nitrogen atoms providing the enhanced Lewis acid–base interactions between MOF framework and Cd^{2+} ions.

Enantiopure MOFs also could be synthesized based on ligand exchange, which can be used for chiral recognition and separation. A pair of homochiral S(R)-ZIF-78 materials were obtained through using S(R)–OH-BIM to selectively exchange the 5-NBIM ligand in **ZIF-78**, although the parent MOF, ZIF-78, was constructed with divalent zinc center and two types of ligands (2-NIM and 5-NBIM) [45]. The ligand exchange reaction was performed by soaking **ZIF-78** in an n-butanol solution of S(R)–OH-BIM at 120 ℃ for 7 days, and the solution was replaced with fresh ones every 24 h during the process. The presence of S(R)–OH-BIM ligands in the resultant MOF materials was proven by ¹H NMR, and the homochirality of S(R)-ZIF-78 h was confirmed by circular dichroism(CD) measurements. The S(R)-ZIF-78 h were potential for chiral recognition and separation of D- and L-proline. The S-ZIF-78 h showed a stronger interaction with L-proline than with D-proline, which was confirmed by a negative Cotton effect of the CD signal when S-ZIF-78 h was added into a racemic mixture of D-proline and L-proline.

During ligand exchange, taking advantage of the time interval after the old coordination bonds break but before the new bonds are formed can realize the encapsulation of some target material in the cages or pores of MOFs. Basnayake and co-workers reported that the encapsulation of red sulfur chromophores inside a microporous ZIF with the SOD topology could be achieved in the process of the transformation of **SIM-1** to **ZIF-8** via ligand exchange in DMF without loss in crystallinity (Fig. 28) [111]. First, the nano crystals of **SIM-1** was prepared through the SALE of **ZIF-8**. Then, the linker exchange of **SIM-1** with 4-methyl-5-imidazolecarboxaldehyde was performed by stirring a mixture anhydrous DMF solution of **SIM-1**, Na_2S_4 and 2-methylimidazole at 100 ℃ for 48 h under N_2 atomosphere. During the exchange process, the aldehyde group of 4-methyl-5-imidazolecarboxaldehyde could accept electrons from the partial sulfides and sulfur radicals to generate elemental sulfur and further lead to the formation of S_4, the red sulfur chromophore. At the same time, the removal of a linker molecule resulted in a temporary defect that allowed sulfur species to be encapsulated. PXRD and SEM characterizations showed that the red solid products had the same crystal structure and morphology as **ZIF-8**. FTIR spectrum confirmed the complete conversion of **SIM-1** to **ZIF-8** by the disappearance of a band at 1656 cm^{-1} corresponding to C = O from the aldehyde groups of the ligands in **SIM-1**. Compared with traditional methods to produce red pigments, entrapping red color sulfur chromophores inside the cages of **ZIF-8** via SALE could avoid the use of toxic heavy metals. These results show that ligand exchange provide a good strategy for encapsulating some useful molecules in MOFs.

Ligand exchange process provides an opportunity for the controlled growth of Au nanowires (Au NWs) in MOFs to achieve
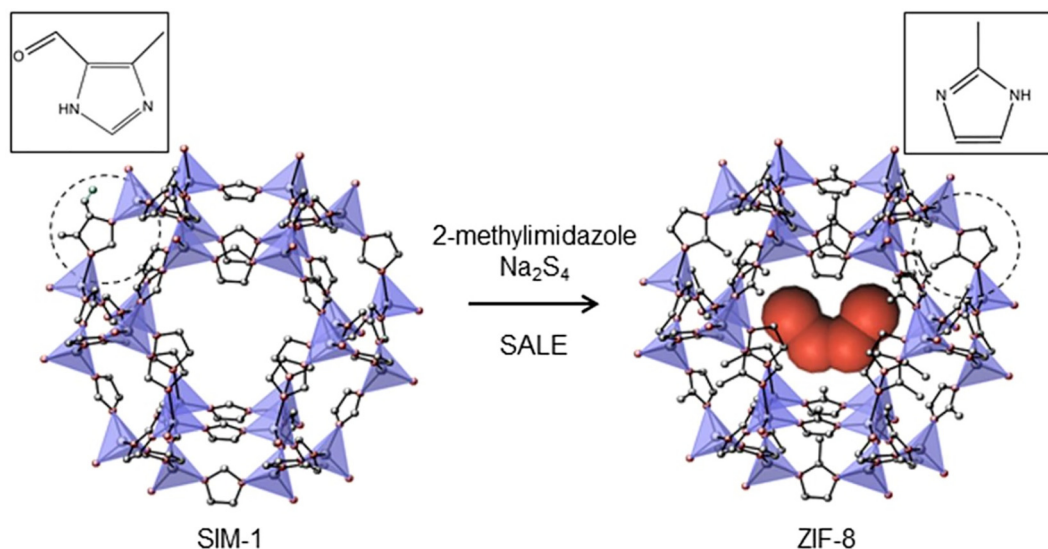

Fig. 28. The cartoon of encapsulation of sulfur species inside **ZIF-8** during SALE from **SIM-1** to **ZIF-8**. Reprinted with permission from Ref. [111].
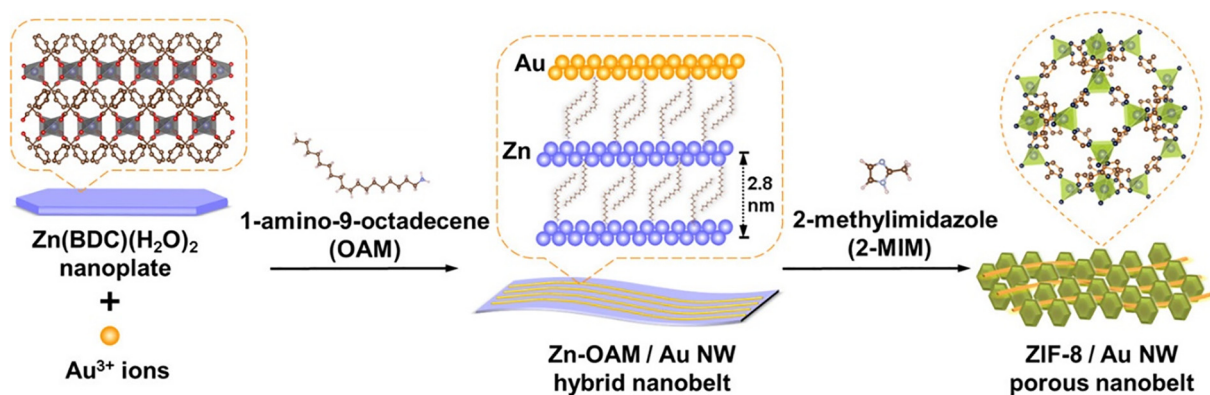
Fig. 29. Schematic illustration of the sequential ligand exchange process of Zn-based polymers for in situ preparation of Zn-OAM/Au NW hybrid nanobelts and ZIF-8/Au NW porous nanobelts. Reprinted with permission from Ref. [112].

enhanced chemical properties of the combined material. Li and co-workers reported the synthesis of nanobelt-type Zn-OAM (OAM = oleylamine) with a well-defined laminar structure through postsynthetic ligand exchange reaction of $Zn(BDC)(H_2O)_2$ [112]. Meanwhile, Au NWs were in situ deposited on the nanobelts,

resulting in a composite, Zn-OAM/Au NW. Furthermore, OAM ligands were exchanged with 2-MIM to form a porous conposite composed of ZIF-8 nanoparticles interwound by Au NWs (ZIF-8/Au NW) (Fig. 29). Compared with the nonresponsive Au NWs or Zn-based polymers alone, Zn-OAM/Au NW and ZIF-8/Au NW

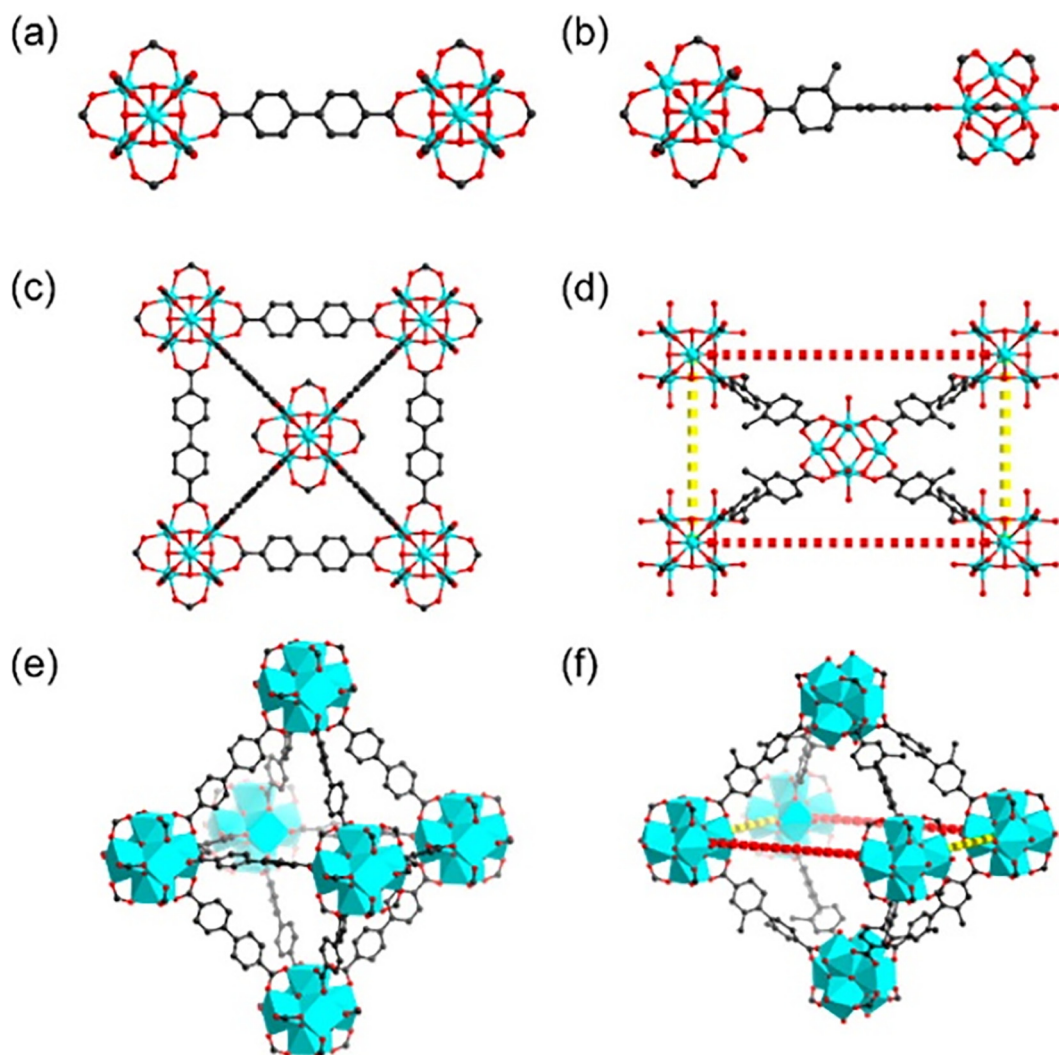**Fig. 30.** (a) Conformation of $BPDC^{2-}$ in the fcu structure. (b) Conformation of Me_2-$BPDC^{2-}$ in the bcu structure. (c, e) fcu structure formed with $BPDC^{2-}$. (d, f) bcu structure formed with Me_2-$BPDC^{2-}$. Reprinted with permission from Ref. [58].
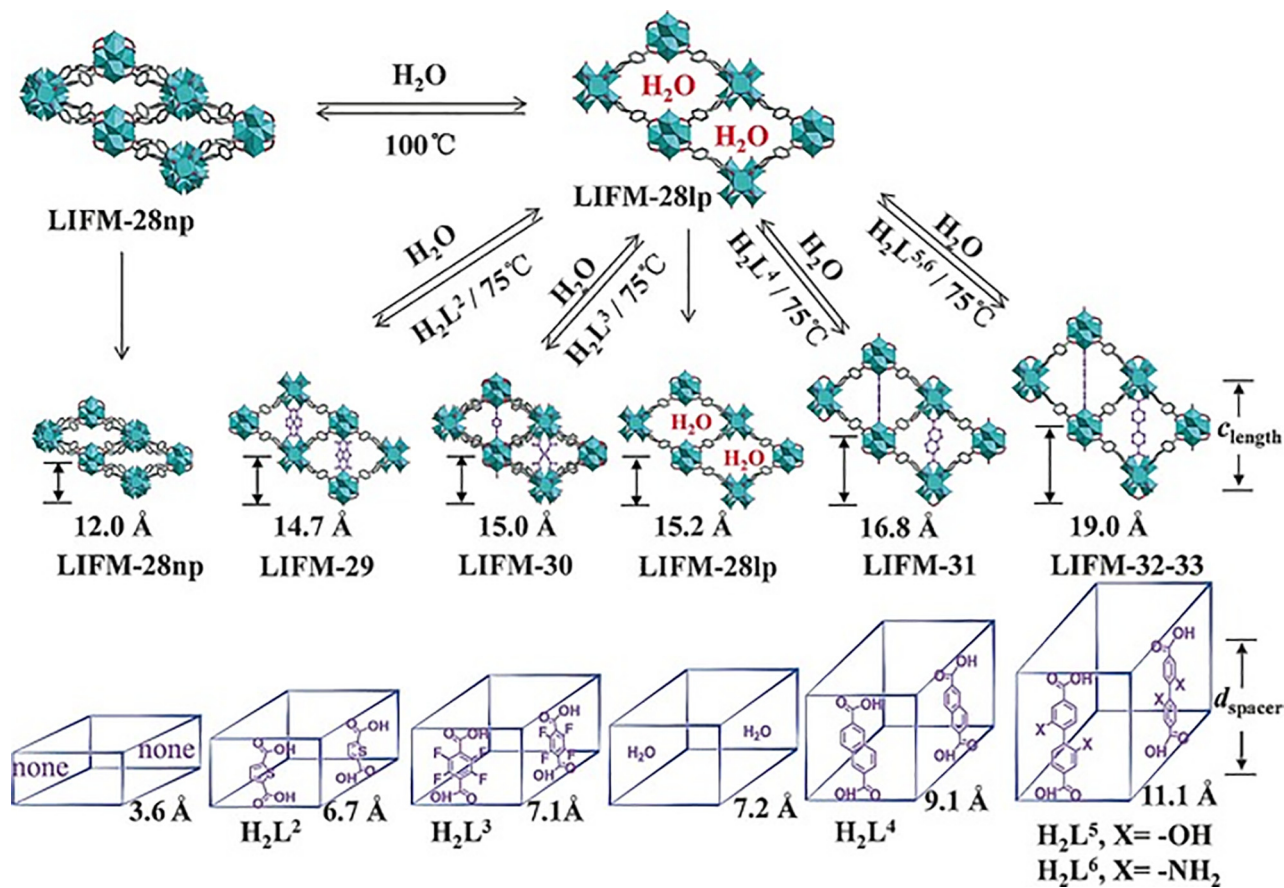
Fig. 31. Reversible breathing behavior of **LIFM-28**, and stepwise installation/ uninstallation of spacers in an increasing sequence of expansion magnitude. Reprinted with permission from Ref. [117].

exhibited good selectivity toward NO_2 in conductive sensing experiments with a limit of detection (LOD) of 760 and 190 ppb, respectively.

4.4. Terminal ligand exchange

Terminal ligands on metal centers can be removed [113] to create open sites for the accommodation of linear bidentate linkers with suitable lengths, and this process can be called terminal ligand exchange. Terminal ligand exchange reactions of 2D and 3D MOFs will be discussed as follows.

The exchange of terminal ligands by bidentate ligand or multidentate ligand could make the structure increased from low dimensional to high dimensional. When the terminal or monodentate ligands in 2D MOFs are exchanged, the dimensions of these MOFs frameworks could be expanded into 3D frameworks. For examples, two 3D MOFs, $[Cd_2(BTX)_2(BDC)_2]_n$ and $[Co_2(BTX)_3 (BDC)_2(H_2O)_2]_n$, were obtained by Huang and co-workers through exchanging the Cl^- ions coordinating with metal centers of two 2D grid-type MOFs, $[Cd(BTX)_2Cl_2]_n$ and $[Co(BTX)_2Cl_2]_n$, with terephthalate anions [81]. Similarly, A 2D MOF, $\{[Zn_3(CPN)_3 (urotropine)_2] \cdot 2DMF \cdot 3H_2O\}_n$ (**1 2 9**), could transform into a 3D MOF, $\{[Zn(CPN)(AZP)] \cdot 4DMF \cdot 2H_2O\}_n$ (**1 3 0**), via replacing the
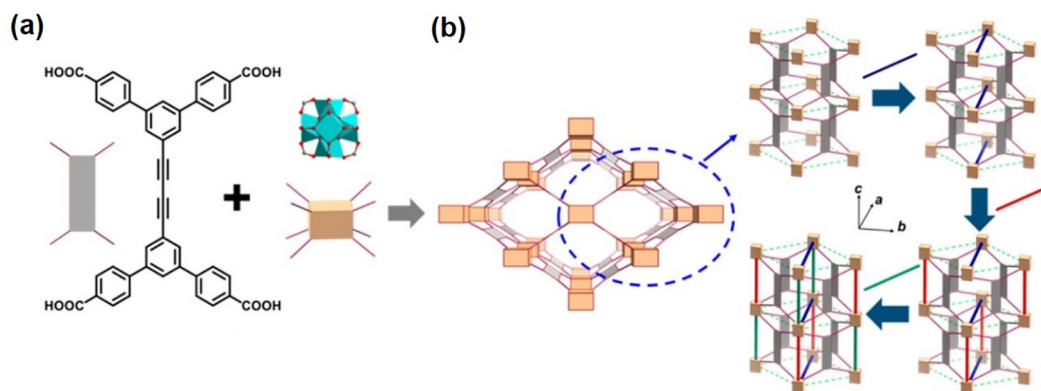

Fig. 32. (a) Primary tetratopic linker and Zr_6 cluster, their topological representation (b) The augmented scu and schematic illustration of the stepwise insertion of three linkers. Adapted with permission from Ref. [119].
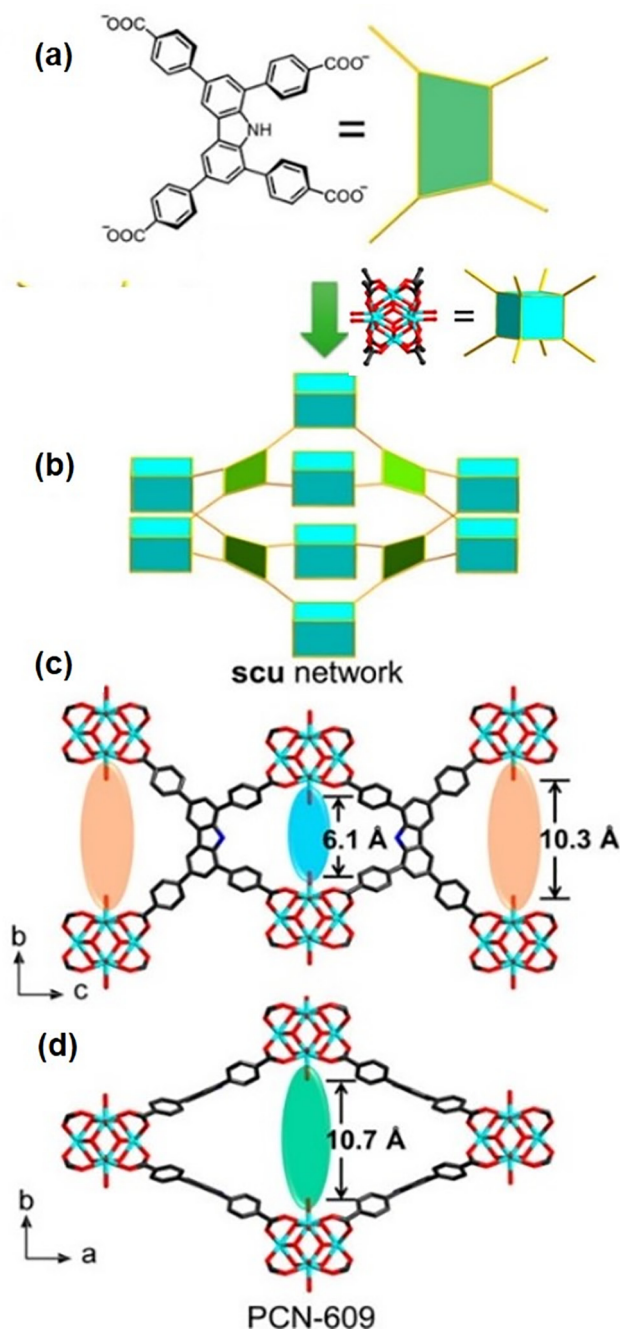
Fig. 33. (a) Biphenyl-based rectangular linker and Zr_6 clusters. (b) Schematic representation of **PCN-609**. Single crystal structure of **PCN-609** viewed along a-direction (c) and c-direction (d). Pocket I, II, and III are colored blue, orange, and green, respectively. Adapted with permission from Ref. [120].

original dangling urotropine ligands with the linear bridging AZP ligands in the SC-SC manner at room temperature. However, it was unexpected that the original trinuclear $[Zn_3(COO)_6]$ SBUs changed to a mononuclear node in the ligand exchange process [114].

When the terminal OH^-/H_2O ligands of metal centers in a 3D MOF are exchanged by linear single-carboxylate or dicarboxylate linkers, phase transformation reaction accompanied by topological change can occur to construct MTV-MOFs with precisely positioned functionalities in the desired proximity [115]. Zhou's group first applied this strategy into **PCN-700** which is constructed with

eight-connected $Zr_6O_4(OH)_8(H_2O)_4$ clusters and Me_2-BPDC^{2-} ligands [58]. The terminal OH^-/H_2O ligands on Zr_6 clusters of the MOF could be exchanged by linear BDC^{2-} and Me_2-BPDC^{2-} which respectively connect two types of adjacent Zr_6 cluster pairs with different distance sizes (two types of pockets) (Fig. 30). Interestingly, the resultant MTV-MOF (**PCN-703**) containing three kinds of ligands of different length could only be obtained by sequential insertion of BDC^{2-} and Me_2-BPDC^{2-} but not by sequential insertion of Me_2-BPDC^{2-} and BDC^{2-}, which indicated that the exchange sequence was important. Similarly, another MTV-MOF **PCN-704** was also obtained by sequential insertion of NH_2-BDC^{2-} and $(CH_3O)_2$-TPDC. Later, guided by a geometrical analysis, 11 new MOFs were constructed from **PCN-700** using the terminal ligand exchange strategy and each had three different ligands in predefined positions [116]. These studies verify that the terminal ligand strategy can achieve systematic variation of the pore volume and decoration of pore environment.

Then, Su's group developed a cost-saving strategy of conducting different MTV-MOFs by using a reused swing-role MOF (**LIFM-28**) in a simple function-change process [117]. **LIFM-28** with two types of pockets between 8-connected Zr_6 clusters was chosen to predictably implement kinetic installation/uninstallation of additional spacers with different lengths and functionality. The pocket along a-axis was rigid, but the other pocket along the c-axis was flexible and could accommodate the insertion of dicarboxylic acid linkers with lengths ranging from 6.7 to 11.1 Å (Fig. 31). The ligand-installed products, **LIFM-29–33** with inserted dicarboxylic acid ligands of different lengths along the c-axis can be obtained by socking **LIFM-28** in the DMF solution of the corresponding ligands, and **LIFM-29–33** also could transform back into **LIFM-28** by immersing them in water for the reuse of parent framework [117]. Later, **LIFM-70–86** with isomorphous structures but variant functional moieties (amine, trifluoromethyl, fluorine, methyl, phenolic hydroxyl, 2,2-bipyridine, Pd-coordinated 2,2-bipyridine, and azide groups) were obtained by the same group via the exchange of terminal OH^-/H_2O ligands on 8-connected Zr_6 clusters with functional bridging linkers of two different lengths. **LIFM-28** could be regained when **LIFM-70–86** were soaked in water for different times through SC-SC transformation, which provides an opportunity for **LIFM-28** to switch among different functional versions for various applications, such as gas separation, catalysis, click reaction, luminescence, and extraordinary methane storage [118].

The complexity of $Zr(IV)$-MOFs can be further enhanced by increasing the types of pockets that can accommodate three or more linear linkers of different lengths. Zhang's group synthesized the MOF, **NPF-300**, constructed with Zr_6 clusters and tetratopic linkers whose conformation could change and produce three types of pockets in the MOF [119]. The three types of pockets could accommodate the stepwise insertion of three different secondary linkers (Fig. 32). The chemical stability of the resulting MOFs after linkers installation are determined by two important factors, size-matching and mechanic strain. In another work, Zhou's and coworkers directly synthesized a $Zr(IV)$-MOF (**PCN-609**) with three types of pockets by using a carbazole-tetracarboxylate linker with Cs point group symmetry and 8-connected Zr_6 clusters [120]. The low-symmetry **PCN-609** was used as a matrix to perform three-step exchanges of terminal OH^-/H_2O ligands with three other ligands with different lengths to construct MTV-MOFs (Fig. 33). Considering the varieties of $Zr(IV)$-MOFs with unsaturated coordination, the strategy of exchanging terminal ligands with various dicarboxylic acid linkers in above works exhibits a great potential in further developing MTV-MOFs.

Fluorescent ligands can be also inserted to enhance the fluorescence of Zr-MOFs through ligand exchange of terminal OH^-/H_2O on 8-connected Zr_6 clusters. A series of fluorescent Zr-MOFs, **LIFM-31/50/51/52/53** were synthesized by Su's group using a
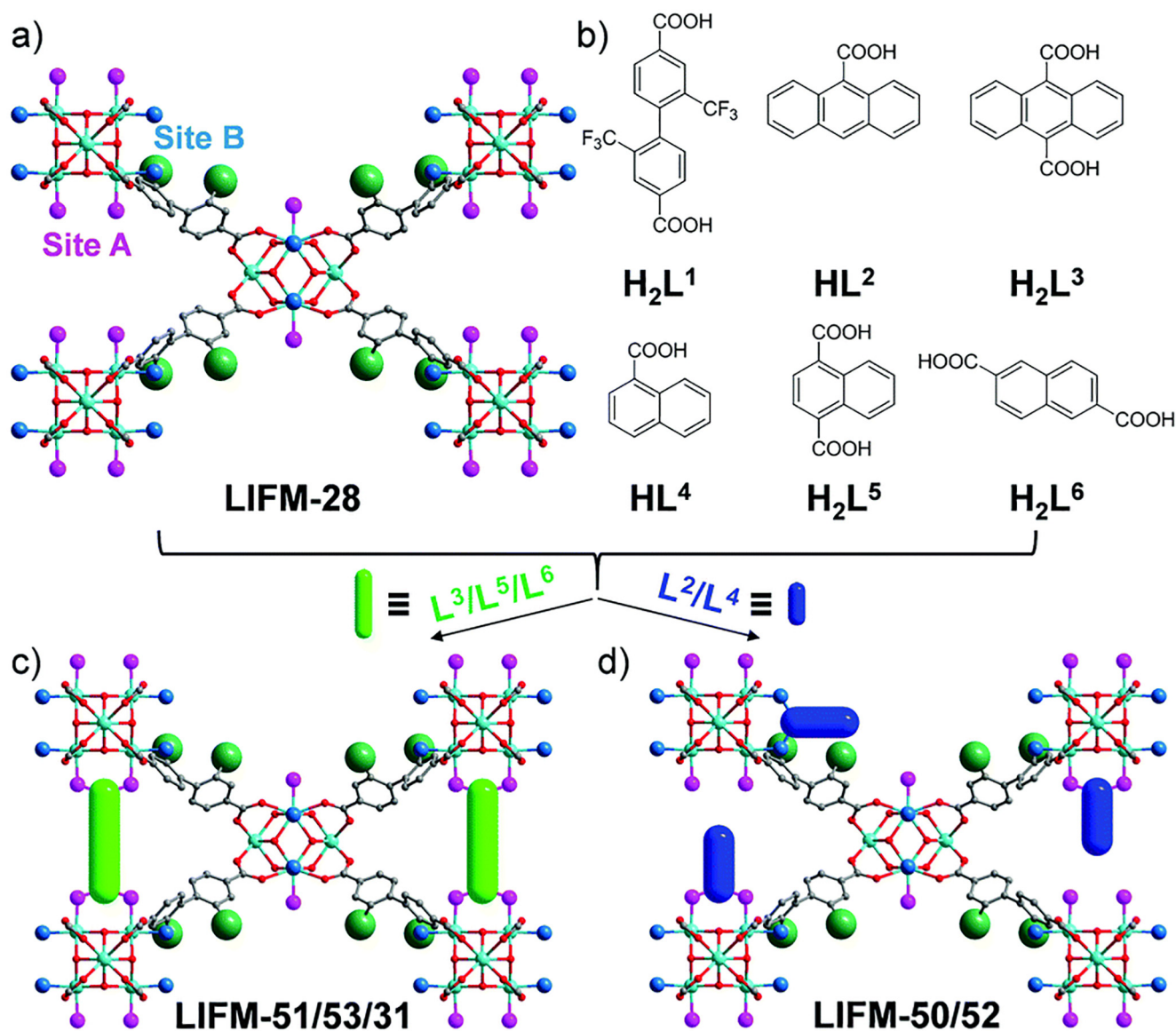
Fig. 34. (a) The structure of **LIFM-28**, (b) the structure of the ligand precursors, (c) MOFs inserted with a dicarboxylate ligand, (d) MOFs inserted with a single carboxylate ligand randomly dangling on the clusters. Reprinted with permission from the Ref. [121].

swing-role LIFM-28 as matrix to accommodate switchable organic ligands as fluorophores (Fig. 34) [121]. The experiments were performed by immersing the pristine LIFM-28 into the DMF solution of the five fluorescent ligands at 75 °C, respectively. The resulting five MOFs showed obvious emission spectra of different wavelength, which indicated that the insertion of different ligands as dominating fluorophores can tune and regulate the emission wavelength of MOFs.

Introducing functional ligands containing metal ions can improve the catalytic performance of MOFs. The MOF PCN-700-BPYDC(Cu)-TPDC^{2-} was prepared by Zhou's group through stepwise terminal OH$^-$/H$_2$O exchange and metalation [116]. The functional MOF can be applied to the size-selective catalytic system for aerobic alcohol oxidation reaction, and the size selectivity of the MOF catalysts could be tuned by changing the substituents (R) (methyl groups, phenyl groups, and hexyl groups) on the TPDC-R$_2^{2-}$ linkers. Later, metallated ligands were introduced in **PCN-160** and by the same group through sequential ligand elim-

ination and terminal OH/H$_2$O exchange with M(Fe^{2+}, Co^{2+}, Ni^{2+}, Cu^{2+}, and Pd^{2+}.)-INA$_2$ [122,123]. First, patical ligand AZDC^{2-} in **PCN-160** was replaced by CBAB^{2-}, then CBAB^{2-} was dissociated into 4-aminobenzoic acid and 4-formylbenzoic acid through hydrolysis by acetic acid/DMF solution to create missing-linker defects. Last, the terminal OH/H$_2$O were exchanged by M−INA$_2$ (Fig. 35). The improved catalytic activities of PCN-160-47%Ni was demonstrated for the ethylene dimerization reaction [68,73]. Later, Cui's group introduced the single- or mixed-metallized ligand into **UiO-68** by direct ligand exchange [124]. The single-M(Cu, V, Mn, Cr, Fe) linker MOFs synthesized by one-step ligand exchange could be used to catalyze asymmetric cyanosilylation of aldehydes, ring-opening of epoxides, oxidative kinetic resolution of secondary alcohols, and aminolysis of stilbene oxide reactions. The mixed-M(Mn-Cr, Mn-V) linker MOFs synthesized by two-step ligand exchange were catalytically active for sequential asymmetric alkene epoxidation/epoxide ring-opening reactions.
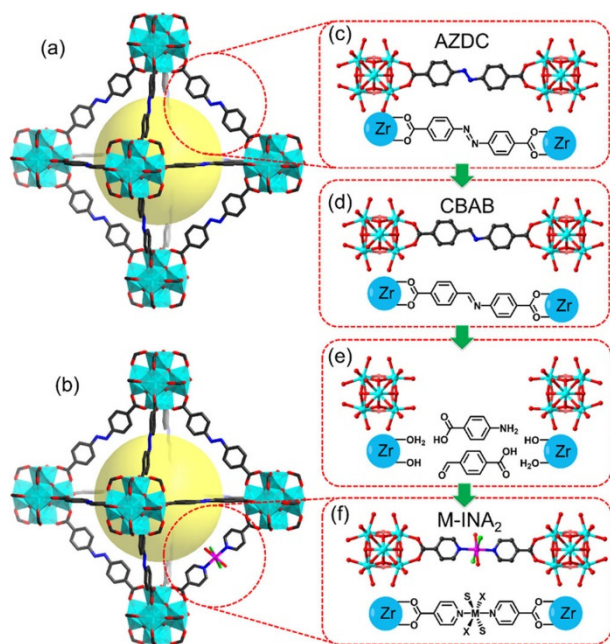
Fig. 35. Structures of **PCN-160** (a) and PCN-160-R%M with transchelating ligands (b). Transformation of ligand fragment in **PCN-160** (c) by CBAB^{2-} exchange (d), linker labialization (e), and installation of M−INA$_2$ (f). Reprinted with permission from Ref. [122].

5. Conclusions and outlook

As a type of tailorable porous materials, MOFs have extensive applications in the fields of gas adsorption, separation, catalysis, sensing, etc. The design and synthesis of novel MOFs is important for their future development in various applications. It is obvious that the exchange of metal ions or ligands in MOFs would be a promising strategy of constructing the desired MOFs that are not accessible by a direct one-pot self-assembly approach and enriching the family of isoreticular MOFs. In addition, the significance of exchange reaction can be fully reflected by the following aspects. 1) Not only the mixed-metal or mixed-ligand MOFs can be constructed, but also the proportion of various metal ions or ligands in MOFs can be effectively adjusted by controlling exchange reaction conditions. 2) Core-shell architectures can be achieved when the exchange reaction proceeds gradually from the external surface into the inner structure of the parent MOF crystals, while homogeneous solid solutions usually are obtained by *de novo synthesis*. 3) Some structural defects (ligand missing or unsaturated metal sites) can be created in the daughter MOFs after the exchange reactions of the parent MOFs, increasing the active sites in daughter MOFs and improving their adsorption/separation or catalytic performance. 4) The purpose of some exchange reactions is not to construct new MOFs, but to achieve adsorption or detection of specific metal ions as incoming ions or to encapsulate some target material in the pores of MOFs by taking advantage of the time interval after the break of old coordination bonds and before the formation of new coordination bonds. The examples of structural design and property modification (stability, hydrophilic/hydrophobic, adsorption/separation, catalytic, fluorescence, magnetic, etc) based on metal ion and ligand exchange in the past five years have been overviewed in this review. It is worth mentioning that much progress has been made in terminal ligand exchange for obtaining MTV-MOFs. In addition, the influencing factors and processes of exchange reactions in MOFs have been summarized and analyzed based on these examples. Unlike traditional synthesis methods, exchange reaction is a process starting from a template with well-defined structure, which is mainly due to the nature of the "labile and reversible" coordination bonds. Thus, when exchange reaction is used to synthesize MOFs, the structures and enhanced properties of novel MOFs are more easily predicted and controlled. There is still large space for further exploration in obtaining MOFs with desired structure and application performance by exchange reactions.

Although there has been some progress in the research about the influencing factors of exchange reaction rate and degree in the past five years, the mechanism of exchange reaction is not fully understood and utilized. Particularly, the exact location of the exchanged metal ions or ligands in the target samples was not studied in depth despite the template MOFs have multiple crystallographically independent metal nodes or ligands. In addition, it should be pointed out that crystal structures of some exchanged products mentioned in section 3 and 4 can not be directly determined by SCXRD measurements, which was due to that their crystal quality became poor through the exchange reactions. In particular, in some cases, the exchanged products may gradually lose their crystallinitycrystalline and change into amorphous powder phases with the prolongation of exchange reaction durationthe for increasing exchange ratio. Therefore, how to keep the crystallinity and integrity of the original crystals in the exchange reactions remains to be further studied. Summarily, it is of great significance to further investigate the exchange reactions of MOFs by experiments or theoretical calculation.

Declaration of Competing Interest

The authors declare that they have no known competing financial interests or personal relationships that could have appeared to influence the work reported in this paper.

Acknowledgements

Appendix A. Supplementary data

Supplementary data to this article can be found online at https://doi.org/10.1016/j.ccr.2020.213421.

References

[1] H.C. Zhou, J.R. Long, O.M. Yaghi, Chem. Rev. 112 (2012) 673–674.
[2] J.R. Long, O.M. Yaghi, Chem. Soc. Rev. 38 (2009) 1213–1214.
[3] T.R. Cook, Y.-R. Zheng, P.J. Stang, Chem. Rev. 113 (2013) 734–777.
[4] Y. Bai, Y. Dou, L.-H. Xie, W. Rutledge, J.-R. Li, H.-C. Zhou, Chem. Soc. Rev. 45 (2016) 2327–2367.
[5] R.-B. Lin, S.-Y. Liu, J.-W. Ye, X.-Y. Li, J.-P. Zhang, Adv. Sci. 3 (2016) 1500434–1500454.
[6] Y. Liu, H. Dong, F. Hu, Y.S. Zhao, Sci. Bull. 62 (2017) 3–4.
[7] H.-C.J. Zhou, S. Kitagawa, Chem. Soc. Rev. 43 (2014) 5415–5418.
[8] T.A. Makal, J.R. Li, W. Lu, H.C. Zhou, Chem. Soc. Rev. 41 (2012) 7761–7779.
[9] J.R. Li, J. Sculley, H.C. Zhou, Chem. Rev. 112 (2012) 869–932.
[10] J.R. Li, R.J. Kuppler, H.C. Zhou, Chem. Soc. Rev. 38 (2009) 1477–1504.
[11] K. Sumida, D.L. Rogow, J.A. Mason, T.M. McDonald, E.D. Bloch, Z.R. Herm, T.-H. Bae, J.R. Long, Chem. Rev. 112 (2012) 724–781.
[12] L. Ma, C. Abney, W. Lin, Chem. Soc. Rev. 38 (2009) 1248–1256.
[13] J. Lee, O.K. Farha, J. Roberts, K.A. Scheidt, S.T. Nguyen, J.T. Hupp, Chem. Soc. Rev. 38 (2009) 1450–1459.
[14] M. Yoon, R. Srirambalaji, K. Kim, Chem. Rev. 112 (2012) 1196–1231.
[15] L.E. Kreno, K. Leong, O.K. Farha, M. Allendorf, R.P. Van Duyne, J.T. Hupp, Chem. Rev. 112 (2012) 1105–1125.

[16] Y. Cui, Y. Yue, G. Qian, B. Chen, Chem. Rev. 112 (2012) 1126–1162.
[17] S. Aguado, J. Canivet, D. Farrusseng, J. Mater. Chem. 21 (2011) 7582–7588.
[18] C.-C. Wang, Y.-S. Ho, Scientometrics 109 (2016) 481–513.
[19] R. Frem, G. Arroyos, J. Flor, R. Alves, G. Lucena, C. Silva, M. Coura, Quim. Nova 41 (2018) 1178–1191.
[20] Y. Han, J.-R. Li, Y. Xie, G. Guo, Chem. Soc. Rev. 43 (2014) 5952–5982.
[21] P. Cui, P. Wang, Y. Zhao, W.-Y. Sun, Cryst. Growth Des. 19 (2019) 1454–1470.
[22] H. Wang, W. Meng, J. Wu, J. Ding, H. Hou, Y. Fan, Coordin. Chem. Rev. 307 (2016) 130–146.
[23] Z. Yin, S. Wan, J. Yang, M. Kurmoo, M.-H. Zeng, Coordin. Chem. Rev. 378 (2019) 500–512.
[24] S.-L. Huang, T.S.A. Hor, G.-X. Jin, Coordin. Chem. Rev. 346 (2017) 112–122.
[25] Y. He, J. Shang, Q. Gu, G. Li, J. Li, R. Singh, P. Xiao, P.A. Webley, Chem. Commun. 51 (2015) 14716–14719.
[26] M. Lalonde, W. Bury, O. Karagiaridi, Z. Brown, J.T. Hupp, O.K. Farha, J. Mater. Chem. A 1 (2013) 5453–5468.
[27] C.K. Brozek, L. Bellarosa, T. Soejima, T.V. Clark, N. Lopez, M. Dinca, Chem. Eur. J. 20 (2014) 6871–6874.
[28] C.K. Brozek, M. Dinca, Chem. Commun. 51 (2015) 11780–11782.
[29] S. Shin, S. Jeong, D. Kim, M.S. Lah, Cryst. Growth Des. 17 (2017) 2228–2237.
[30] J.-Y. Wu, C.-J. Tsai, C.-Y. Chang, Y.-Y. Wu, J. Solid State Chem. 246 (2017) 23–28.
[31] D.F. Sava Gallis, M.V. Parkes, J.A. Greathouse, X. Zhang, T.M. Nenoff, Chem. Mater. 27 (2015) 2018–2025.
[32] C.-W. Tsai, J.W. Niemantsverdriet, E.H.G. Langner, Micropor. Mesopor. Mat. 262 (2018) 98–105.
[33] C.K. Brozek, M. Dinca, Chem. Soc. Rev. 43 (2014) 5456–5467.
[34] J.D. Evans, C.J. Sumby, C.J. Doonan, Chem. Soc. Rev. 43 (2014) 5933–5951.
[35] P. Kumar, A. Pournara, K.-H. Kim, V. Bansal, S. Rapti, M.J. Manos, Prog. Mater. Sci. 86 (2017) 25–74.
[36] Y. Noori, K. Akhbari, RSC Adv. 7 (2017) 1782–1808.
[37] Y.-F. Niu, W. Zhao, J. Han, X.-L. Zhao GeTian, Cryst. Eng. Comm. 16 (2014) 2344–2347.
[38] J. Yang, X. Wang, F. Dai, L. Zhang, R. Wang, D. Sun, Inorg. Chem. 53 (2014) 10649–10653.
[39] X. Liu, C. Hao, J. Li, Y. Wang, Y. Hou, X. Li, L. Zhao, H. Zhu, W. Guo, Inorg. Chem. Front. 5 (2018) 2898–2905.
[40] J. Li, Y. Fan, Y. Ren, J. Liao, C. Qi, H. Jiang, Inorg. Chem. 57 (2018) 1203–1212.
[41] K.S. Asha, R. Bhattacharjee, S. Mandal, Angew. Chem. Int. Ed. 55 (2016) 11528–11532.
[42] F.L. Zhang, J.Q. Chen, L.F. Qin, L. Tian, Z. Li, X. Ren, Z.G. Gu, Chem. Commun. 52 (2016) 4796–4799.
[43] M.B. Lalonde, J.E. Mondloch, P. Deria, A.A. Sarjeant, S.S. Al-Juaid, O.I. Osman, O.K. Farha, J.T. Hupp, Inorg. Chem. 54 (2015) 7142–7144.
[44] L. Huang, M. He, B. Chen, B. Hu, J. Mater. Chem. A 4 (2016) 5159–5166.
[45] C. Zhuo, F. Wang, J. Zhang, Cryst. Eng. Comm. 20 (2018) 5925–5928.
[46] P. Wang, K. Chen, Q. Liu, H.W. Wang, M. Azam, S.I. Al-Resayes, Y. Lu, W.Y. Sun, Dalton Trans. 46 (2017) 11425–11430.
[47] H. Fei, S.M. Cohen, J. Am. Chem. Soc. 137 (2015) 2191–2194.
[48] J. Park, D. Feng, H.C. Zhou, J. Am. Chem. Soc. 137 (2015) 1663–1672.
[49] P. Deria, J.E. Mondloch, O. Karagiaridi, W. Bury, J.T. Hupp, O.K. Farha, Chem. Soc. Rev. 43 (2014) 5896–5913.
[50] M.Y. Masoomi, A. Morsali, A. Dhakshinamoorthy, H. Garcia, Angew. Chem. Int. Ed. 58 (2019) 15188–15205.
[51] S. Abednatanzi, P. Gohari Derakhshandeh, H. Depauw, F.X. Coudert, H. Vrielinck, P. Van Der Voort, K. Leus, Chem. Soc. Rev. 48 (2019) 2535–2565.
[52] L. Li, H. Xue, Y. Wang, P. Zhao, D. Zhu, M. Jiang, X. Zhao, A.C.S. Appl. Mater. Interfaces 7 (2015) 25402–25412.
[53] L.W. Lee, Y.C. Kao, M.Y. Chung, B.C. Chang, G.H. Lee, S.M. Peng, C.M. Wang, Y.H. Liu, S.L. Lee, K.L. Lu, Dalton Trans. 48 (2019) 1950–1954.
[54] P.P. Cui, X.D. Zhang, P. Wang, Y. Zhao, M. Azam, S.I. Al-Resayes, W.Y. Sun, Inorg. Chem. 56 (2017) 14157–14163.
[55] U. Fluch, V. Paneta, D. Primetzhofer, S. Ott, Chem. Commun. 53 (2017) 6516–6519.
[56] K.C. Jayachandrababu, D.S. Sholl, S. Nair, J. Am. Chem. Soc. 139 (2017) 5906–5915.
[57] J.A. Boissonnault, A.G. Wong-Foy, A.J. Matzger, J. Am. Chem. Soc. 139 (2017) 14841–14844.
[58] S. Yuan, W. Lu, Y.P. Chen, Q. Zhang, T.F. Liu, D. Feng, X. Wang, J. Qin, H.C. Zhou, J. Am. Chem. Soc. 137 (2015) 3177–3180.
[59] C. Liu, C. Zeng, T.Y. Luo, A.D. Merg, R. Jin, N.L. Rosi, J. Am. Chem. Soc. 138 (2016) 12045–12048.
[60] G. Gonzalez Miera, A. Bermejo Gomez, P.J. Chupas, B. Martin-Matute, K.W. Chapman, A.E. Platero-Prats, Inorg. Chem. 56 (2017) 4577–4584.
[61] C. Liu, T.Y. Luo, E.S. Feura, C. Zhang, N.L. Rosi, J. Am. Chem. Soc. 137 (2015) 10508–10511.
[62] S. Sen, S. Neogi, K. Rissanen, P.K. Bharadwaj, Chem. Commun. 51 (2015) 3173–3176.
[63] N. Zhao, F. Sun, H. He, J. Jia, G. Zhu, Cryst. Growth Des. 14 (2014) 1738–1743.
[64] Z. Xiao, Y. Wang, S. Zhang, W. Fan, X. Xin, X. Pan, L. Zhang, D. Sun, Cryst. Growth Des. 17 (2017) 4084–4089.
[65] J. Park, D. Feng, H.C. Zhou, J. Am. Chem. Soc. 137 (2015) (1809) 11801–11811.
[66] O. Karagiaridi, W. Bury, J.E. Mondloch, J.T. Hupp, O.K. Farha, Angew. Chem. Int. Ed. 53 (2014) 4530–4540.
[67] X. Cui, A.N. Khlobystov, X. Chen, D.H. Marsh, A.J. Blake, W. Lewis, N.R. Champness, C.J. Roberts, M. Schroder, Chem. Eur. J. 15 (2009) 8861–8873.
[68] X.-F. Zhang, T. Yan, T. Wang, J. Feng, Q. Wang, X. Wang, L. Du, Q.-H. Zhao, Crystengcomm 20 (2018) 570–577.
[69] T. Grancha, J. Ferrando-Soria, H.C. Zhou, J. Gascon, B. Seoane, J. Pasan, O. Fabelo, M. Julve, E. Pardo, Angew. Chem. Int. Ed. 54 (2015) 6521–6525.
[70] Y. Xu, N.A. Vermeulen, Y. Liu, J.T. Hupp, O.K. Farha, Eur. J. Inorg. Chem. (2016) 4345–4348.
[71] S.A.A. Razavi, A. Morsali, Chem. Eur. J. 25 (2019) 10876–10885.
[72] A.W. Stubbs, L. Braglia, E. Borfecchia, R.J. Meyer, Y. Román- Leshkov, C. Lamberti, M. Dincă, ACS Catal. 8 (2017) 596–601.
[73] Y.-J. Hu, J. Yang, Y.-Y. Liu, S. Song, J.-F. Ma, Cryst. Growth Des. 15 (2015) 3822–3831.
[74] S. Bommakanti, U. Venkataramudu, S.K. Das, Cryst. Growth Des. 19 (2018) 1155–1166.
[75] S. Bommakanti, S.K. Das, CrystEngComm 21 (2019) 2438–2446.
[76] A.M. Wright, A.J. Rieth, S. Yang, E.N. Wang, M. Dinca, Chem. Sci. 9 (2018) 3856–3859.
[77] Z. Shao, C. Huang, J. Dang, Q. Wu, Y. Liu, J. Ding, H. Hou, Chem. Mater. 30 (2018) 7979–7987.
[78] M. Yadollahi, H. Hamadi, V. Nobakht, Appl. Organometal. Chem. 33 (2019) e4819–e4830.
[79] H. Wang, C. Huang, Y. Han, Z. Shao, H. Hou, Y. Fan, Dalton Trans. 45 (2016) 7776–7785.
[80] A. Margariti, S. Rapti, A.D. Katsenis, T. Friščić, Y. Georgiou, M.J. Manos, G.S. Papaefstathiou, Inorg. Chem. Front. 4 (2017) 773–781.
[81] S. Huang, X. Li, X. Shi, H. Hou, Y. Fan, J. Mater. Chem. 20 (2010) 5695–5699.
[82] O. Karagiaridi, W. Bury, D. Fairen-Jimenez, C.E. Wilmer, A.A. Sarjeant, J.T. Hupp, O.K. Farha, Inorg. Chem. 53 (2014) 10432–10436.
[83] G. Minguez Espallargas, E. Coronado, Chem. Soc. Rev. 47 (2018) 533–557.
[84] S.S. Nadar, V.K. Rathod, Int. J. Biol. Macromol. 120 (2018) 2293–2302.
[85] P. Deria, J.E. Mondloch, E. Tylianakis, P. Ghosh, W. Bury, R.Q. Snurr, J.T. Hupp, O.K. Farha, J. Am. Chem. Soc. 135 (2013) 16801–16804.
[86] G. Ferey, C. Serre, C. Mellot-Draznieks, F. Millange, S. Surble, J. Dutour, I. Margiolaki, Angew. Chem. Int. Ed. 43 (2004) 6296–6301.
[87] A. Sonnauer, F. Hoffmann, M. Froba, L. Kienle, V. Duppel, M. Thommes, C. Serre, G. Ferey, N. Stock, Angew. Chem. Int. Ed. 48 (2009) 3791–3794.
[88] X. Lian, D. Feng, Y.P. Chen, T.F. Liu, X. Wang, H.C. Zhou, Chem. Sci. 6 (2015) 7044–7048.
[89] J.H. Wang, Y. Zhang, M. Li, S. Yan, D. Li, X.M. Zhang, Angew. Chem. Int. Ed. 56 (2017) 6478–6482.
[90] B. Wang, Q. Yang, C. Guo, Y. Sun, L.-H. Xie, J.-R. Li, Acs Appl. Mater. Inter. 9 (2017) 10286–10295.
[91] T. He, Y.-Z. Zhang, X.-J. Kong, J. Yu, X.-L. Lv, Y. Wu, Z.-J. Guo, J.-R. Li, Acs Appl. Mater. Inter. 10 (2018) 16650–16659.
[92] M.M. Xu, X.J. Kong, T. He, X.Q. Wu, L.H. Xie, J.R. Li, Inorg. Chem. 57 (2018) 14260–14268.
[93] C.X. Yang, H.B. Ren, X.P. Yan, Anal. Chem. 85 (2013) 7441–7446.
[94] Y. Zhou, H.-H. Chen, B. Yan, J. Mater. Chem. A 2 (2014) 13691–13697.
[95] X.S. Wang, L. Li, D. Li, J. Ye, Sol. RRL (2020) 1900547–1900581.
[96] W. Lin, H. Frei, J. Am. Chem. Soc. 127 (2005) 1610–1611.
[97] R. Nakamura, A. Okamoto, H. Osawa, H. Irie, K. Hashimoto, J. Am. Chem. Soc. 129 (2007) 9596–9597.
[98] H. Han, H. Frei, J. Phys. Chem. C 112 (2008) 8391–8399.
[99] D. Sun, W. Liu, M. Qiu, Y. Zhang, Z. Li, Chem. Commun. 51 (2015) 2056–2059.
[100] T.-F. Liu, L. Zou, D. Feng, Y.-P. Chen, S. Fordham, X. Wang, Y. Liu, H.-C. Zhou, J. Am. Chem. Soc. 136 (2014) 7813–7816.
[101] D. De, S. Neogi, E.C. Sanudo, P.K. Bharadwaj, Chem. Eur. J. 21 (2015) 17422–17429.
[102] M.Y. Masoomi, M. Bagheri, A. Morsali, Cryst. Eng. Comm. 19 (2017) 5749–5754.
[103] P. Mahata, S. Natarajan, P. Panissod, M. Drillon, J. Am. Chem. Soc. 131 (2009) 10140–10150.
[104] H. Furukawa, K.E. Cordova, M. O'Keeffe, O.M. Yaghi, Science 341 (2013) 1230444–1230458.
[105] N. Yanai, T. Uemura, M. Inoue, R. Matsuda, T. Fukushima, M. Tsujimoto, S. Isoda, S. Kitagawa, J. Am. Chem. Soc. 134 (2012) 4501–4504.
[106] M. Taddei, R.J. Wakeham, A. Koutsianos, E. Andreoli, A.R. Barron, Angew. Chem. Int. Ed. 57 (2018) 11706–11710.
[107] O. Karagiaridi, N.A. Vermeulen, R.C. Klet, T.C. Wang, P.Z. Moghadam, S.S. Al-Juaid, J.F. Stoddart, J.T. Hupp, O.K. Farha, Inorg. Chem. 54 (2015) 1785–1790.
[108] U. Fluch, B.D. McCarthy, S. Ott, Dalton Trans. 48 (2019) 45–49.
[109] A. Phan, C.J. Doonan, F.J. Uribe-Romo, C.B. Knobler, M. O'keeffe, A.O.M. Yaghl, Accounts Chem. Res. 43 (2010) 58–67.
[110] J.Q. Jiang, C.X. Yang, X.P. Yan, Chem. Commun. 51 (2015) 6540–6543.
[111] S.A. Basnayake, K. Tan, M. Leonard, Y. Chabal, K.J. Balkus, Micropor. Mesopor. Mat. 219 (2016) 172–177.
[112] P. Li, H. Zhan, S. Tian, J. Wang, X. Wang, Z. Zhu, Y. Dai, Z. Wang, C. Zhang, X. Huang, W. Huang, A.C.S. Appl. Mater. Interfaces 11 (2019) 13624–13631.
[113] P. Deria, W. Bury, J.T. Hupp, O.K. Farha, Chem. Commun. 50 (2014) 1965–1968.
[114] V. Sharma, D. De, S. Pal, P. Saha, P.K. Bharadwaj, Inorg. Chem. 56 (2017) 8847–8855.
[115] L. Feng, K.Y. Wang, G.S. Day, H.C. Zhou, Chem. Soc. Rev. 48 (2019) 4823–4853.
[116] S. Yuan, Y.P. Chen, J.S. Qin, W. Lu, L. Zou, Q. Zhang, X. Wang, X. Sun, H.C. Zhou, J. Am. Chem. Soc. 138 (2016) 8912–8919.
[117] C.X. Chen, Z. Wei, J.J. Jiang, Y.Z. Fan, S.P. Zheng, C.C. Cao, Y.H. Li, D. Fenske, C.Y. Su, Angew. Chem. Int. Ed. 55 (2016) 9932–9936.

[118] C.X. Chen, Z.W. Wei, J.J. Jiang, S.P. Zheng, H.P. Wang, Q.F. Qiu, C.C. Cao, D. Fenske, C.Y. Su, J. Am. Chem. Soc. 139 (2017) 6034–6037.
[119] X. Zhang, B.L. Frey, Y.S. Chen, J. Zhang, J. Am. Chem. Soc. 140 (2018) 7710–7715.
[120] J. Pang, S. Yuan, J. Qin, M. Wu, C.T. Lollar, J. Li, N. Huang, B. Li, P. Zhang, H.C. Zhou, J. Am. Chem. Soc. 140 (2018) 12328–12332.
[121] C.X. Chen, Q.F. Qiu, M. Pan, C.C. Cao, N.X. Zhu, H.P. Wang, J.J. Jiang, Z.W. Wei, C.Y. Su, Chem. Commun. 54 (2018) 13666–13669.
[122] S. Yuan, P. Zhang, L. Zhang, A.T. Garcia-Esparza, D. Sokaras, J.S. Qin, L. Feng, G. S. Day, W. Chen, H.F. Drake, P. Elumalai, S.T. Madrahimov, D. Sun, H.C. Zhou, J. Am. Chem. Soc. 140 (2018) 10814–10819.
[123] S. Yuan, L. Zou, J.S. Qin, J. Li, L. Huang, L. Feng, X. Wang, M. Bosch, A. Alsalme, T. Cagin, H.C. Zhou, Nat. Commun. 8 (2017) 15356–15366.
[124] C. Tan, X. Han, Z. Li, Y. Liu, Y. Cui, J. Am. Chem. Soc. 140 (2018) 16229–16236.
[125] X. Zhao, Z. Zhang, X. Cai, B. Ding, C. Sun, G. Liu, C. Hu, S. Shao, M. Pang, ACS Appl. Mater. Interfaces 11 (2019) 7884–7892.